Plateaus and jumps in the atmospheric radiocarbon record – Potential origin and value as global age markers for glacial-to-deglacial paleoceanography, a synthesis

Michael Sarnthein[1)], Kevin Küssner[2)], Pieter M. Grootes[3)], Blanca Ausin[4)8)], Timothy Eglinton[8)], Juan Muglia[5)], Raimund Muscheler[6)], Gordon Schlolaut[7)]

1) Institute of Geosciences, University of Kiel, Olshausenstr. 40, 24098 Kiel, Germany, michael.sarnthein@ifg.uni-kiel.de, (corresponding author)
2) Alfred-Wegener-Institut Helmholtz-Zentrum für Polar- und Meeresforschung, Department for Marine Geology, 27570 Bremerhaven, Germany, kevin.kuessner@awi.de
3) Institute of Ecosystem Research, University of Kiel, Olshausenstr. 40, 24098 Kiel, Germany, pgrootes@ecology.uni-kiel.de
4) Geology Department, University of Salamanca, Plaza de los Caldos, 37008 Salamanca, Spain, <ausin@usal.es>
5) Centro para el Estudio de los Sistemas Marinos, CONICET, 2915 Boulevard Brown, U9120ACD, Puerto Madryn, Argentina, jmuglia@cenpat-conicet.gob.ar
6) Quaternary Sciences, Department of Geology Lund University, Sölvegatan 12, 22362 Lund, Sweden, raimund.muscheler@geol.lu.se
7) Climate Dynamics and Landscape Evolution, GFZ German Centre for Geosciences, Telegrafenberg, 14473 Potsdam, Germany, SchlolautG@gmail.com
8) Geological Institute, ETH Zürich, Sonneggstr. 5, 8092 Zuerich, Switzerland,

final version submitted to CLIMATE OF THE PAST (2020-6-12)

ABSTRACT

Changes in the geometry of ocean Meridional Overturning Circulation (MOC) are crucial in controlling changes of climate and the carbon inventory of the atmosphere. However, the accurate timing and global correlation of short-term glacial-to-deglacial changes of MOC in different ocean basins still present a major challenge. A possible solution is offered by the fine structure of jumps and plateaus in the record of radiocarbon (^{14}C) concentration of the atmosphere and surface ocean that reflects changes in atmospheric ^{14}C production, ocean-atmosphere ^{14}C exchange, and ocean mixing. Boundaries of atmospheric ^{14}C plateaus in the ^{14}C record of Lake Suigetsu, now tied to Hulu U/Th model-ages instead of optical varve counts, provide a stratigraphic 'rung ladder' of ~30 age tie points from 29 to 10 cal. ka for correlation with and dating of planktic oceanic ^{14}C records. The age differences between contemporary planktic and atmospheric ^{14}C plateaus give an estimate of the global distribution of ^{14}C reservoir ages for surface waters of the Last Glacial Maximum (LGM) and deglacial Heinrich Stadial 1 (HS-1), as shown by about 20 planktic ^{14}C records. Clearly elevated and variable reservoir ages mark both upwelling regions and high-latitude sites covered by sea ice and/or meltwater. ^{14}C ventilation ages of LGM deep waters reveal opposed geometries of Atlantic and Pacific MOC. Similar to today, Atlantic deep-water formation went along with an estuarine inflow of old abyssal waters from the Southern Ocean up to the northern North Pacific and an outflow of upper deep waters. Vice versa, ^{14}C ventilation ages suggest a reversed MOC during early HS-1 and a ~1500 year-long flushing of the deep North Pacific up to the South China Sea, when estuarine circulation geometry marked the North Atlantic, gradually starting near 19 ka. Elevated ^{14}C ventilation ages of LGM deep waters reflect a major drawdown of carbon from the atmosphere. The subsequent, massive age drop and related change in MOC induced major events of carbon release to the atmosphere as recorded in Antarctic ice cores. These new features of MOC and the carbon cycle provide detailed evidence in terms of space and time needed to test and refine ocean models that, in part because of insufficient spatial model resolution and reference data for testing the model results, still poorly reproduce them.

1. INTRODUCTION

1.1 A variety of terms linked to the notion '^{14}C age'

The ^{14}C concentration in the troposphere is mainly determined by ^{14}C production, atmospheric mixing, moreover, air-sea gas exchange, and ocean circulation that vary over time (e.g., Alves et al., 2018; Alveson et al., 2018). The ^{14}C content of living terrestrial plants is in equilibrium with the atmosphere via processes of photosynthesis and respiration, and accordingly, the ^{14}C of terrestrial plant remains in a sediment section directly reflects the amount of radioactive decay, thus the time passed since the plant's death, and the ^{14}C composition of the atmosphere during the time of plant growth.

Contrariwise, ^{14}C values of marine and inland waters are cut off from cosmogenic ^{14}C production in the atmosphere, hence depend on the carbon transfer at the air-water interface and the result of local transport and mixing of carbon in the water. For surface waters, the air-sea transfer is relatively fast and effective involving a time span of ten years and less (e.g., Nydal et al., 1998). Yet, vertical and horizontal water mixing results in surface ocean ^{14}C concentrations on average 5 % lower than those in the contemporaneous atmosphere, a difference expressed as 'Marine Reservoir Age' (or 'reservoir effect' *sensu* Alves et al., 2018). These 'ages' reflect the local oceanography and are highly variable through time. They may range from near zero up to values of more than 700 yr, in some regions up to 2500 yr, induced, for example, by old waters upwelled from below (e.g., Stuiver and Braziunas, 1993; Grootes and Sarnthein, 2006; Sarnthein et al., 2015). Apart from U/Th dated corals (many papers on their reservoir age since Adkins and Boyle, 1997) the ^{14}C age of planktic foraminifers is the most common tracer of surface water ages in marine sediments, a rough estimate of the time passed since sediment deposition. Initially, marine geologists were most interested in this ‘simple’ age value. Soon, however, they were confronted with age inconsistencies that implied a series of unknowns, in particular the ^{14}C ‘reservoir age’ that finally became a most valuable tracer for oceanography.

In turn, ^{14}C records of benthic foraminifers in deep-sea sediments reflect the time of radioactive decay since their deposition with the apparent ‘ventilation age’ of the deep waters in which they lived. Ventilation age is primarily the time span from the moment when carbon dissolved in the (later) deep waters lost contact with the atmosphere and the somewhat reduced ^{14}C level of surface waters until the precipitation of benthic carbonate. Details on the derivation of ventilation ages are provided in Cook and Keigwin (2015) and Balmer and Sarnthein (2018). In addition, however, ventilation ages depict hardly quantifiable lateral admixtures of older and/or younger water masses, moreover, ^{14}C-enriched organic carbon supplied by the biological pump, thus are called ‘apparent’. Today, the apparent transit times of carbon dissolved in the deep ocean range from a few hundred up to ~1800 ^{14}C yr found in upper deep waters of the northeastern North Pacific (Matsumoto, 2007).

Over the last decades, it turned out that both the reservoir ages of surface waters and the ventilation ages of deep waters present robust and high-resolution tracers essential for drawing quantitative conclusions on past ocean circulation geometries, marine climate change, and the processes that drive both past ocean dynamics and carbon budgets, given the ages rely on a number of robust age tie points. Obtaining such tie points presents a problem, since any attempt to date a deep-sea sediment record by means of ^{14}C encounters a number of intricacies of how to disentangle the effects of global atmospheric ^{14}C variations due to past changes in cosmogenic ^{14}C production and carbon cycle from (i) local depositional effects such as sediment hiatuses and winnowing, differential bioturbational mixing depth, and sediment transport by deep burrows, (ii) the effects of local atmosphere-ocean exchange and ocean mixing resulting in reservoir and ventilation ages that change through time and space (e.g., Alves et al. 2018; Grootes and Sarnthein, 2006), and (iii) from the final target, quantitatively 'pure' ^{14}C ages due to radioactive decay. These problems are exacerbated by the need for a generally accepted high-precision atmospheric reference record for the period 14–50 cal. ka, beyond tree ring calibration,

By now, ^{14}C-based chronologies of deep-sea sediment records, used to constrain and correlate the age of glacial-to-deglacial changes in ocean dynamics and climate on a global scale, are often of unsatisfactory quality when they are based on (i) age tie points spaced far too wide (e.g., using DO-events 1, 2, and 3 only and/or sporadic tephra layers for the time span 30–14 cal ka), (ii) disregarding atmospheric ^{14}C plateaus, (iii) the risky assumption of ±constant planktic ^{14}C reservoir ages and other speculative stratigraphic correlations/compilations, and (iv) ignoring small-scale major differences in low-latitude reservoir age. Likewise, clear conclusions are precluded by an uncertainty range of 3-4 kyr sometimes accepted for tie points during the glacial-to-deglacial period (Stern and Lisiecki, 2013; Lisiecki and Stern, 2016), where significant global climate oscillations occurred on decadal-to-centennial time scales as widely shown on the basis of speleothem and ice core-based records (Steffensen et al., 2008; Svensson et al., 2008; Wang et al., 2001).

Thus marine paleoclimate and paleoceanographic studies today focus on the continuing quest for a high-resolution and global, hence necessarily atmospheric ^{14}C reference record that is marked by abundant, narrow-standing tie points on the calibrated (cal.) age scale. Such pertinent tie points are provided by a suite of reproducible ‘plateaus’ and ‘jumps’ that mark the atmospheric ^{14}C record (Figs. 1 and S1; Sarnthein et al., 2007 and 2015; Bronk Ramsey et al., 2012 and 2019; Schlolaut et al., 2018; Umling and Thunnell, 2017), hence form the basis of this synthesis.

1.2 Review of tie points used to fix calibrated and reservoir ages in marine ^{14}C records

The tree ring-based calibration of ^{14}C ages provides a master record of decadal changes in atmospheric ^{14}C concentrations back to ~14 cal. ka (Reimer et al., 2013 and 2020) with floating sections beyond (from ~12.5–14.5 cal. ka and around 29–31.5 and 43 cal. ka; Turney et al., 2010, 2017, Reimer et al., 2020). The evolution of Holocene and late deglacial ^{14}C ages with time is not linear but reveals variations with numerous distinct jumps (= rapid change) and (short) plateau-shaped (slow or no change or even inversion) structures indicative of fluctuations in atmospheric ^{14}C concentration. Prior to 8500 cal. yr BP, various plateaus extend over 400–600 cal. yr and beyond (Fig. 2). Given the quality of the tree ring calibration data, these fluctuations can be considered real, suitable for global correlation (Sarnthein et al., 2007, 2015; Sarnthein and Werner, 2018). Air-sea gas exchange transfers the atmospheric ^{14}C fluctuations into the surface ocean where they can provide high-resolution tie points to calibrate the marine ^{14}C record and marine reservoir ages back to ~14 ka (via the so-called ^{14}C wiggle match approach). In the near future, however, it is unlikely that a continuous tree ring-based record will become available to trace such atmospheric ^{14}C variations further back, over the period 14–29 cal. ka crucial for the understanding of last-glacial-to-interglacial changes in climate. Hence various other, less perfect ^{14}C archives have been employed for this period to tie past changes in atmospheric ^{14}C concentration/age to an ‘absolute’ or ’calibrated’ (e.g., incremental and/or based on speleothem carbonate) age scale. This record can then be used to constrain the widely unknown evolution of ^{14}C reservoir ages of surface waters for various regions of the ocean.

Suites of ^{14}C ages of paired marine and terrestrial plant-borne samples, e.g. paired planktic foraminifers and wood chunks, provide most effective but rarely realizable absolute-age markers and reservoir ages of local ocean surface waters (Zhao and Keigwin, 2018; Rafter et al., 2018; Schroeder et al., 2016; Broecker et al., 2004). Likewise successful appears the alignment of ^{14}C-dated variations in downcore sea-surface temperatures (SST) with changes in hydroclimate as recorded in age-calibrated sedimentary leaf-wax hydrogen isotope (δD) records from ancient lakes (Muschitiello et al., 2019), assumed to be coeval. Further tie points are derived from volcanic ash layers (Waelbroeck et al., 2001; Siani et al, 2013; Davies et al., 2014; Sikes and Guilderson, 2016), paired U/Th- and ^{14}C-based coral ages (Adkins and Boyle, 1997; Robinson et al., 2005; Burke and Robinson, 2012; Chen et al., 2015), and the (fairly fragmentary) alignment of major tipping points in ^{14}C dated records of marine SST and planktic $\delta^{18}O$ to the incremental age scale of climate events dated in polar ice core records (Waelbroeck et al., 2011). Such well-defined tie points, however, are wide-spaced in peak glacial-to-early deglacial ice core records, too wide for properly resolving a clear picture of the spatiotemporal pattern of marine paleoclimate events. Finally, various data compilations tentatively rely on the use of multiple age correlations amongst likewise poorly dated marine sediment records, an effort necessarily problematic.

Skinner et al. (2019) recently combined new and existing reservoir age estimates from North Atlantic and Southern Ocean to show coherent but distinct regional reservoir age trends in subpolar ocean regions, trends that indeed envelop the range of actual major small-scale and short-term oscillations in reservoir age revealed by our technique of ^{14}C plateau tuning for the subpolar South Pacific (Küssner et al., in prep.).

In the absence of robust age tie points an increasing number of authors resort to ^{14}C reservoir age simulations for various sea regions by ocean General Circulation Models (GCM) (e.g. Butzin et al., 2017; Muglia et al., 2018) to quantify the potential difference between marine and atmospheric ^{14}C dates during glacial-to-interglacial times. Considering the complexity of the ocean MOC and the global carbon cycle it is not surprising that the results of a comparison of a selection of robust empiric vs. simulated ^{14}C reservoir ages are not that encouraging yet (as discussed further below).

Accepting a generally close link between ^{14}C concentrations in the troposphere and in the surface ocean, the fine structure of planktic ^{14}C records with centennial-scale-resolution provides far superior (though costly) evidence, similar to that of tree rings, to furnish a series of age tie points with semi-millennial-scale time resolution for a global correlation of glacial-to-deglacial marine sediment sections. These suites of tie structures can link the marine sediment records to a reference suite of narrow-standing jumps and boundaries of the apparent plateaus robustly identified in the atmospheric ^{14}C record of Lake Suigetsu, the only long, continuous record based on terrestrial plant remains (Bronk Ramsey et al., 2012, 2019) provided that common ^{14}C variations are robustly identified in both atmospheric and marine records. Prior to the reach of the tree ring-based age scale ~14 cal. ka, the absolute age of these atmospheric ^{14}C structures can be either calibrated by incremental (microscopy- or XRF-based) varve counts (Schlolaut et al., 2018; Marshall et al., 2012) or by a series of paired U/Th- and ^{14}C-based model ages correlated from the Hulu Cave speleothem record (Bronk Ramsey, 2012 and 2019; Southon et al., 2012; Cheng et al., 2018). The difference between these calibrations (Fig. 3) is discussed below. The difference, however, is of little importance neither for the tuning of planktic to corresponding atmospheric ^{14}C plateaus nor for the derivation of planktic reservoir ages that present the highly variable offset of the ^{14}C age of a planktic plateau from that of the correlated atmospheric plateau. The offset is deduced by subtracting the average ^{14}C age of an atmospheric ^{14}C plateau from that of the correlated planktic ^{14}C plateau, independent of any absolute age value assigned.

A basic philosophical controversy exists whether the apparent jump and plateau structures in the Suigetsu and planktic ^{14}C records reflect real ^{14}C fluctuations or statistical noise. In the 'null hypothesis' the ^{14}C values shaping plateaus of the calibration curve are regarded as result of mere statistical scatter. Thus, the record of atmospheric ^{14}C ages against time would form a simple continuous rise resulting from radioactive decay and the advance of time, such as suggested by a fairly straight progression of the highly resolved deglacial Hulu Cave ^{14}C record plotted vs. U/Th ages (Southon et al., 2012; Cheng et al., 2018).

This null hypothesis is contradicted by the 'master record' of tree ring data (Fig. 2; Reimer et al., 2013 /2020). Unequivocally it shows fluctuations in atmospheric ^{14}C concentration on the order of 2–3 % over the last 10 kyr (Stuiver and Braziunas, 1993) and even larger back to ~14 ka (Reimer et al., 2013, 2020). Though not resolved in speleothem data these plateau/jump structures most likely are real and widely reproducible in marine sediment records. Under glacial and deglacial low-CO_2 conditions beyond 14 ka, when climate and ocean dynamics were less constant than during the Holocene, atmospheric ^{14}C fluctuations were, most likely, even stronger than those reported by Stuiver and Braziunas and ^{14}C plateaus and jumps accordingly larger. Also, plateau-jump structures are becoming increasingly evident in the evolving atmospheric calibration record (Reimer et al., 2020).

Thus, the age-defined plateaus and jumps in the Suigetsu atmospheric ^{14}C calibration curve may most likely be regarded as a suite of ‘real’ structures, extending the tree ring record for Holocene and B/A-to-Early Holocene times (Fig. 2) into early deglacial and LGM times. In part the plateau/jump structures may be linked to changes in cosmogenic ^{14}C production, as possibly shown in the ^{10}Be record (Fig. 4; based on data of Adolphi et al., 2018), and – presumably more dominant – to short-term changes in ocean mixing and the carbon exchange between ocean and atmosphere. The exchange is crucial, since the carbon reservoir of the ocean contains up to 60 (preindustrial) atmospheric carbon units (Berger and Keir, 1984). The apparent contradiction with the smooth Hulu Cave ^{14}C record (Southon et al., 2012; Cheng et al., 2018) may possibly be explained by the Hulu Cave speleothem precipitation system acting as a low-pass filter for fluctuating atmospheric ^{14}C concentrations (statistical tests of Bronk Ramsey et al., pers. comm. 2018) and, to a very limited degree, by the obvious scatter in the Suigetsu data. That scatter, however, appears insufficient to feign plateaus in view of the evidence based on tree ring-based plateaus (Fig. 2). The filter for Hulu data possibly led to a loss especially of short-lived structures in the preserved atmospheric ^{14}C record, though some remainders were preserved in the ^{14}C records of Hulu Cave (Fig. 1). So we rather trust in the amplitude of Suigetsu ^{14}C structures, but trust in the timing of Hulu

Cave data as discussed below. We prefer the Suigetsu record to IntCal, since it is based on original primary atmospheric data and results in small-scale spatio-temporal changes of reservoir age, whereas IntCal is mixing and smoothing a broad array of different data sources with comparatively coarse age resolution, including carbonate-based speleothem and marine records.

Like a ‘rung ladder’ the age-calibrated suite of ^{14}C plateau boundaries and jumps is suited for tracing the calibrated age of numerous plateau boundaries in glacial-to-deglacial marine ^{14}C records likewise densely sampled, even when some rungs have been destroyed by local influences on gas exchange or ocean mixing. Also, one may record the average offset of planktic ^{14}C ages from paired atmospheric ^{14}C ages, i.e. the planktic reservoir age, for each single ^{14}C plateau (Sarnthein et al., 2007, 2015). For the first time, this suite of tie points may facilitate a precise temporal correlation of all sorts of changes in surface and deep-water composition on a global scale, crucial for a better understanding of past changes in ocean and climate dynamics.

1.3 Items discussed in this synthesis

The Results Section summarizes (1) some means to separate noise, global atmospheric and local oceanic forcings, that jointly control the structure of a planktic ^{14}C age-depth curve. (2) The choice of a U/Th-based reference time scale (Bronk Ramsey et al. 2012; Cheng et al., 2018) instead of the earlier varve-counted version (Schlolaut et al., 2018) to date the structures in the global atmospheric ^{14}C record of Lake Suigetsu (Sarnthein et al., 2015). (3) An extension of the suite of age tie points from 23 back to 29 cal. ka, values crucial for an accurate global correlation of ocean events over the period 10–29 cal. ka. (4) Potential linkages of atmospheric ^{14}C plateaus and jumps to cosmogenic ^{14}C production and/or ocean dynamics.

The Discussion and Implications section includes the following topics:
(1) A global summary of published marine ^{14}C reservoir age records (Sarnthein et al. 2015) now enlarged by nine plateau-tuned records from the Southern Hemisphere and northeast Atlantic plus three wood chunk-based records (Broecker et al., 2004; Zhao et al., 2018).
(2) A comparison of our plateau-based reservoir ages with independent model-based LGM estimates of surface water ^{14}C reservoir ages. This includes a discussion of habitat- and season-specific ^{14}C reservoir ages characteristic of different planktic foraminifera species, that monitor past changes in the local geometry of surface ocean dynamics (Sarnthein and Werner, 2018).
(3) More detailed insights into the origin of past changes in the global carbon cycle from glacial to interglacial times are provided by the enlarged set of ^{14}C reservoir and ventilation ages that form a robust tracer of global circulation geometries and the inorganic carbon (DIC) dissolved in different basins of the ocean (Sarnthein et al., 2013).

In this way we highlight the important role the technique of ^{14}C plateau tuning and its revised cal. time scale are playing for global data-model intercomparison and a new understanding of Ocean MOC during the LGM and its reversal during HS-1.

2. RESULTS – AGE TIE POINTS BASED ON ^{14}C PLATEAU BOUNDARIES

2.1 *Suite of planktic ^{14}C plateaus: Means to separate global atmospheric from local oceanographic forcings*

The basic assumption of the ^{14}C plateau tuning technique is that the fine structure of fluctuations of the global atmospheric ^{14}C concentration record can also be found in the surface ocean. In a plot of ^{14}C age versus calendar age such fluctuations lead to a pattern of plateaus/jumps that correspond to decreases/increases in ^{14}C concentration. Here we refer to the derivation and interpretation of planktic ^{14}C plateaus, assuming a predom-inantly global atmospheric origin with occasional local oceanographic forcings. The series of planktic ^{14}C plateaus and jumps are derived in cores with average hemipelagic sedimentation rates of >10 cm/ky and dating resolution of <100-150 yr. The plateau-specific structures in a sediment age-depth record form a well-defined suite for which absolute age and reservoir age are derived by means of a strict alignment to the reference suite of global atmospheric ^{14}C plateaus as a whole. Initially, age tie points of planktic foraminiferal $\delta^{18}O$ records showing (orbital) isotope stages #1-3 serve as stratigraphic guideline for the alignment under the simplifying assumption that stratigraphic gaps are absent, not always true (Suppl. Fig. 2). Planktic reservoir ages and their short-term changes are derived from the difference in average ^{14}C age between atmosphere and surface waters in subsequent plateaus. To stick as close as possible to the modern range of reservoir ages (Stuiver and Braziunas, 1993), tuned reservoir ages are kept at a minimum unless stringent evidence requires otherwise.

A close correspondence between ^{14}C concentrations in atmosphere and surface ocean is expected based on rapid gas exchange. In several cases, however, the specific structure and relative length of a planktic ^{14}C plateau may deviate from those of the pertinent plateau observed within the suite of atmospheric plateaus, thus indicate local intra-plateau changes of reservoir age. Though less frequent, these changes may indeed amputate and/or deform a plateau, then as result of variations in local ocean atmosphere exchange and oceanic mixing. Two aspects help to sort out short-term climate-driven intra- and inter-plateau changes in ^{14}C reservoir age: (i) The evaluation of the structure and reservoir age of an individual plateau is strictly including the age estimates deduced for the complete suite of plateaus. (ii) Our experience shows that deglacial climate regimes in control of changes in surface ocean dynamics generally occurred on (multi-) millennial time scales (e.g., YD, B/A, HS-1), whereas atmospheric ^{14}C plateaus hardly lasted longer than a few hundred up to 1100 yr (Fig. 1 and S1). Abrupt changes in gas exchange or ocean mixing usually affect one or only a few plateaus of the suite. -- Absolute age estimates within a plateau are derived by linear interpolation between the age of the base and top of an undisturbed plateau assuming constant sedimentation rates. The potential impact of short-term sedimentation pulses on ^{14}C plateau formation has largely been discarded by Balmer and Sarnthein (2016).

2.2 Suigetsu atmospheric ^{14}C record: Shift to a chronology based on U/Th model ages

Originally, we based the chronology of ^{14}C plateau boundaries in the Suigetsu record (Sarnthein et al., 2015) on a scheme of varve counts by means of light microscopy of thin sections (Bronk Ramsey et al., 2012; Schlolaut et al., 2018). Over the crucial sediment sections of the Last Glacial Maximum (LGM) and deglacial Heinrich Stadial 1 (HS-1), however, varve quality / perceptibility in the Suigetsu profile is highly variable (Fig. 5). In parallel, varve-based age estimates were derived from counting various elemental peaks in µXRF data and interpreted as seasonal signals (Marshall et al., 2012). The results obtained from the two independent counting methods and their interpolations widely support each other but diverge for older ages. The varve counts ultimately formed the backbone of a high-resolution chronology obtained by tying the Suigetsu ^{14}C record to the U/Th based time scale of the Hulu cave ^{14}C record (Bronk Ramsey et al., 2012). Recently, Schlolaut et al. (2018) amended the scheme of varve counts. Accordingly, Suigetsu varve preservation (i.e., the number of siderite layers per 20 cm thick sediment section) is fairly high prior to ~32 ky BP and over late glacial Termination I but fairly poor over large parts of the LGM and HS-1, from ~15 – 32 cal ka (17.3-28.5 m c.d. in Fig. 5). Here only less than 20-40 % of the annual layers expected from interpolation between clearly varved sections are distinguished by microscopy. Varve counts that use µXRF data (Marshall et al., 2012) can distinguish subtle changes in seasonal element variations, that are not distinguishable in thin section microscopy, hence result in higher varve numbers especially during early deglacial-to-peak glacial times. Yet, some subtle variations are difficult to distinguish from noise, which adds uncertainty to the µXRF-based counts. Thus, the results from either counting method are subject to uncertainties that rise with increased varve age (Fig. 5).

Bronk Ramsey et al. (2012) established a third time scale based on ^{14}C wiggle matching to U/Th dated ^{14}C records of the Hulu Cave and Bahama speleothems. In part, this calibrated (cal.) age scale was based on Suigetsu varve counts, in part on the prerequisite of the best-possible fit of a pattern of low-frequency changes in ^{14}C concentration obtained from Suigetsu and Hulu Cave. The two ^{14}C records were fitted within the uncertainty envelope of the Hulu 'Old / Dead Carbon Fraction' (OCF/DCF) of ^{14}C concentration. The uncertainty of this model is still incompletely understood. The U/Th-based age model of Suigetsu may suffer from the wiggle matching of atmospheric ^{14}C ages of Lake Suigetsu with ^{14}C ages of the Hulu Cave (Southon et al., 2012) in case of major short-term changes in atmospheric ^{14}C concentration due to a memory effect of soil organic carbon in carbonate-free regions of the cave overburden. The speleothem-carbonate-based Hulu ages may have been influenced far more strongly by short-term changes in the local DCF than assumed, as suggested by major variations in a paired $\delta^{13}C$ record, that reach up to 5 ‰, mostly subsequent to short-term changes in past monsoon climate (Kong et al., 2005). The uncertainty regarding the assumption of a constant OCF/DCF (Southon et al. 2012; Cheng et al., 2018) may hamper the age model correlation between Hulu and Suigetsu records and the Suigetsu chronology.

We compared the results of the two timescales, independently deduced from varve counts, with those of the U/Th-based model age scale using as test case the base of ^{14}C Plateau 2b, the oldest tie point constrained by µXRF-based counts. In contrast to 16.4 cal. ka, supposed by optical varve counts, µXRF-based counts suggest an age of ~16.9 cal. ka (Marshall et al., 2012; Schlolaut et al., 2018), which matches closely the U/Th-based estimate of 16.93 ka. This is a robust argument for the use of the U/Th-based Suigetsu time scale as 'best possible' age scale to calibrate the age of thirty ^{14}C plateau boundaries (Fig. 1). In its older part, the U/Th model time scale is further corroborated by a decent match of short-term increases in ^{14}C concentration with the low geomagnetic intensity of the Mono Lake and Laschamp events at ~34 and 41.1±0.35 ka (Lascu et al., 2016), independently dated by other methods. The new U/Th-based model ages of ^{14}C plateau boundaries are significantly higher than our earlier microscopy-based varve ages over HS-1 and LGM, a difference increasing from ~200 yr near 15.3 cal. ka to ~530 near 17 ka and 2000 yr near ~29 ka (Fig. 3).

Note, any readjustment of the calendar age of a ^{14}C plateau boundary does not entail any change in ^{14}C reservoir ages afore deduced for surface waters by means of the plateau technique (Sarnthein et al., 2007, 2015), since each reservoir age presents the simple difference in average ^{14}C age for one and the same ^{14}C plateau likewise defined in both the Suigetsu atmospheric and planktic ^{14}C records of marine surface waters, independent of the precise position of this plateau on the calendar age scale.

In view of the recent revision of time scales (Schlolaut et al., 2018; Bronk Ramsey et al, 2019) we now extended our plateau tuning and now also defined the boundaries and age ranges of ^{14}C plateaus and jumps for the interval ~23–29 cal. ka, which results in a total of ~30 atmospheric age tie points for the time span 10.5–29 cal. ka (Fig. 1; summary in Table 1; following the rules of Sarnthein et al., 2007 and 2015). Prior to 25 cal. ka, the definition of ^{14}C plateaus somewhat suffered from an enhanced scatter of raw ^{14}C values of Suigetsu. -- In addition to visual inspection, the ^{14}C jumps and plateaus were also defined with higher statistical objectivity by means of the first-derivative of all trends in the ^{14}C age-to-calendar age relationship (or –core depth relationship, respectively) by using a running kernel window (Sarnthein et al., 2015).

2.3 Linkages of short-term structures in the atmospheric ^{14}C record to changes in cosmogenic ^{14}C production versus changes in ocean dynamics

Potential sources of variability in the atmospheric ^{14}C record have first been discussed by Stuiver and coworkers in the context of Holocene fluctuations deduced from tree ring data (e.g., Stuiver and Braziunas 1993), more recently simulated (e.g., Hain et al., 2014). -- Similar to changes in ^{14}C, variations in ^{10}Be deposition in ice cores reflect past changes in ^{10}Be production as a result of changes in solar activity and the strength of the Earth’s magnetic field (Adolphi et al., 2018). If we accept to omit assumptions on the modulation of past ^{14}C concentrations by changes in the global carbon cycle we can calculate the atmospheric ^{14}C changes over last glacial-to-deglacial times with ^{10}Be and a carbon cycle model and convert them into ^{14}C ages (Fig. 4). Changes in climate and carbon cycle, however, over this period necessarily modified the ^{10}Be-based ^{14}C record if included correctly into the modeling. Between 10 and 13.5 cal. ka, the ^{10}Be-modeled ^{14}C record displays a number of plateau structures that appear to match the Suigetsu-based atmospheric ^{14}C plateaus. Between 15 and 29 cal. ka, however, ^{10}Be-based ^{14}C plateaus are more rare and/or less pronounced than those in the Suigetsu record. Most modelled plateaus are far shorter than those displayed in the suite of atmospheric ^{14}C plateaus of Lake Suigetsu (e.g., plateaus near to the top 2a, 2b, top 5a, and 9), except for a distinct equivalent of plateau no. 6a. On the whole, the modelled and observed structures show little coherence. This may indicate that any direct relationship between variations in cosmogenic ^{14}C production and the Suigetsu plateau record is largely obscured by the carbon cycle, uncorrected climate effects on the ^{10}Be deposition, and/or noise in the ^{14}C data. Also, a relatively high uncertainty of the measured ^{10}Be concentrations in the ice, (in many cases ~7%; Raisbeck et al., 2017), and a lower sample resolution in the order of 50 to 200 yr may contribute to the smoothed character of the ^{10}Be record in Fig. 4.

On the other hand, the 'new' U/Th-based cal. ages of plateau boundaries may suggest some reasonable stratigraphic correlations between peak glacial and deglacial change in atmospheric CO_2 and ^{14}C plateaus with millennial-scale events in paleoceanography (Fig. 6, Table 2): The suite of deglacial ^{14}C plateaus no. 2a, 1, and Top YD indeed displays a temporal match with three brief but major deglacial jumps in ocean degassing of CO_2 documented in the WDC ice core (Marcott et al., 2014). The two records have been independently dated by means of annual-layer counts in ice cores and U/Th ages of stalagmites. The match suggests that these atmospheric ^{14}C plateaus may largely result from changes in air-sea gas exchange, and in turn, from changes in ocean dynamics.

In particular, these events may have been linked to a variety of fast changes such as in sea ice cover in the Southern Ocean and/or in the salinity and buoyancy of high-latitude surface waters (Skinner et al., 2010; Burke and Robinson, 2012). These factors control upwelling and meridional overturning of deep waters, in particular found in the Southern Ocean (Chen et al., 2015) and/or North Pacific (Rae et al. 2014, Gebhardt et al., 2008). Such events of changes in MOC geometry and intensity may be responsible for ocean degassing and the ^{14}C plateaus. The enhanced mixing of the Southern Ocean and a similar, slightly later mixing event in the North Pacific (MD02-2489; Fig. S2d) may have triggered – with phase lag – two trends in parallel, (1) a rise in atmospheric CO_2, in part abrupt (*sensu* Chen et al., 2015; Menviel et al., 2018), and (2) a gradual enrichment in ^{14}C depleted atmospheric carbon, reflected as ^{14}C plateau.

Plateau 6a matches a ^{14}C plateau deduced from atmospheric ^{10}Be concentrations, thus suggests changes in ^{14}C production. Other changes in atmospheric ^{14}C (plateaus 4 and 8) match short-term North Atlantic warmings during peak glacial and earliest deglacial times, similar to that at the end of HS-1 and during plateau 'YD', hence may reflect minor changes in ocean circulation and ocean-atmosphere exchange without major degassing of old ^{14}C depleted deep waters in the North Atlantic (Table 2, Fig. S2a). There is still little information, however, on the origin of several other peak glacial ^{14}C plateaus 17.5–29 cal. ka. The actual linkages of these plateaus to events in ocean MOC still remain to be uncovered.

3. DISCUSSION and IMPLICATIONS

3.1 ^{14}C plateau boundaries – A suite of narrow-spaced age tie points to rate short-term changes in marine sediment budgets, chemical inventories, and climate 29–10 cal. ka

In continuation of previous efforts (Sarnthein et al., 2007 and 2015) the tuning of high-resolution planktic ^{14}C records of ocean sediment cores to the new age-calibrated atmospheric ^{14}C plateau boundaries now makes it possible to establish a 'rung ladder' of ~30 age tie points covering the time span 29 – 10 cal. ka. These global tie points have a time resolution of several hundred to thousand years, and can be used to constrain the chronology and potential leads and lags of events that occurred during peak glacial and deglacial times (Fig. 1). The locations of the 18 (20) cores are shown in Fig. 7. The time histories of the benthic and planktic reservoir ages are summarized in Figs. 8 and S2 and the information these provide is discussed below.

Six prominent examples showing the power and value of additional information obtained by means of the ^{14}C plateau-tuning method are:

(i) The timing of ocean signals of the onset of deglaciation (sudden depletion of planktic $\delta^{18}O$ and rise in SST) in the North Atlantic and North Pacific can now be distinguished in detail from those in the Southern Hemisphere, where warming began at 17.6 cal. ka, when the cooling of Heinrich 1 started in the North Atlantic (Fig. S2) (Küssner et al., in prep.); in harmony with Schmittner and Lund, 2015), a finding important to further constrain global 'bipolar see-saw' (Stocker and Johnsen, 2003).

(ii) Likewise, the end of the cooling equated with the Antarctic Cold Reversal (ACR; WDC Project Members, 2013) in Pacific surface waters off Central Chile was found precisely coeval with the onset of the Younger Dryas cold spell in the Northern Hemisphere (Küssner et al., in prep.).

(iii) Signals of local deep-water formation in the subpolar North Pacific can now be separated from signals originating in the North Atlantic (Rae et al. 2014; Sarnthein et al., 2013). In this way we now can specify and tie major short-lasting reversals in Atlantic and Pacific MOC on a global scale.

(iv) Signals of deglacial meltwater advection can now be distinguished from short-term interstadial warmings in the northern subtropical Atlantic, which helps to locate meltwater outbreaks far beyond the well-known Heinrich belt of ice-rafted debris (Balmer and Sarnthein, 2018).

(v) As outlined above, the timing of marine ^{14}C plateaus can now be compared in detail with that of deglacial events of climate and the atmospheric CO_2 rise independently dated by means of ice core-based stratigraphy (Table 2; Fig. 6). These linkages offer a tool to explore details of deglacial changes in deep-ocean MOC once the suite of ^{14}C plateaus has been properly tuned at any particular ocean site.

(vi) The refined scale of age tie points also reveals unexpected details for changes in the sea ice cover of high latitudes as reflected by anomalously high ^{14}C reservoir ages (e.g. north of Iceland and near to the Azores Islands) and for the evolution of Asian summer monsoon in the northern and southern hemisphere as reflected by periods of reduced sea surface salinity (e.g., Sarnthein et al., 2015; Balmer et al., 2018).

Finally, the plateau-based high-resolution chronology has led to the detection of numerous millennial-scale hiatuses (e.g., Sarnthein et al., 2015; Balmer et al., 2016; Küssner et al., in prep.) overlooked by conventional, e.g., *AnalySerie*-based methods (Paillard et al. 1996) of stratigraphic correlation (Fig. S2). In turn, the hiatuses give intriguing new insights into past changes of bottom current dynamics linked to different millennial-scale geometries of overturning circulation and climate change such as in the South China Sea (Sarnthein et al., 2013 and 2015), in the South Atlantic (Balmer et al. 2016) and southern South Pacific (Ronge et al., 2019).

Clearly, the new atmospheric ^{14}C 'rung ladder' of closely-spaced chronostratigraphic tie points has evolved to a valuable tool to uncover functional chains in paleoceanography, that actually have controlled events of climate change over glacial-to-deglacial times. The extension of the age range back to 29 ka allows constraining potential changes in the ocean dynamics expected for Dansgaard Oeschger (DO) events 2, 3, and 4 as compared to those found for DO-1, though pertinent core records are still missing.

3.2 Observed vs. model-based ^{14}C reservoir ages that act as tracer of past changes in surface ocean dynamics provide incentive for model refinements

Radiocarbon plateau tuning of marine sediment sections to the Suigetsu ^{14}C atmospheric master record allows us to establish at semi-millennial-scale resolution the difference between the average ^{14}C age of coeval atmospheric and planktic ^{14}C plateaus. The suite of changing ^{14}C reservoir ages over time forms a prime tracer of past ocean dynamics influencing local surface waters and a data set crucial to deduce past apparent deep-water ventilation ages (e.g., Muglia et al., 2018; Cook and Keigwin, 2015; Balmer and Sarnthein, 2018).

To better constrain the water depth of past reservoir ages we dated monospecific planktic foraminifera (Sarnthein et al., 2007); in low-to-mid latitudes on *G. bulloides*, *G.*

ruber, or *G. sacculifer* with habitat depths of 0–80/120 m (Jonkers and Kucera, 2017) and in high latitudes, mostly on *N. pachyderma* (s) living at 0–200 m depth (Simstich et al., 2003). Averaging of ^{14}C ages within a ^{14}C plateau helps to remove analytical noise and minor real ^{14}C fluctuations. Nine plateaus are located in the LGM, 18–27 cal. ka (Fig. 1). Here, planktic foraminifera-based reservoir ages show analytical uncertainties of >200 to >300 yr each for standard AMS dating. By comparison, short-term temporal variations in reservoir age reach 200–400 yr, occasionally up to 600 yr, in particular, close to the end of the LGM (Table 3).

To better decode the informative value of our ^{14}C reservoir ages for late LGM we compared average ages of ^{14}C Plateaus 4-5 (18.6–20.9 cal. ka) with estimates generated by various global ocean models, an approach similar to that of Toggweiler et al. (2019) applied to modern reservoir ages of the global ocean. In an earlier paper (Balmer et al., 2016) we compared our empiric reservoir ages for the LGM with GCM-based estimates of Franke et al. (2008) and Butzin et al. (2012). Franke et al. (2008) underestimated our mid-latitude values by up to ~2000 ^{14}C yr, while LGM reservoir age estimates of Butzin et al. (2012) were more consistent with ours. Their GCM considered more realistic boundary conditions such as the LGM freshwater balance in the Southern Ocean and, in particular, LGM SST and wind fields plus the gas transfer velocity for the exchange of ^{14}C of CO_2 (Sweeney et al., 2007). Initially we also planned a continuation of these intercomparison tests with our present, enlarged data set. The results were not encouraging and we were advised by Butzin (pers. com. 2019, Butzin et al., 2020) to wait for a revised GCM capable to resolve more properly the details of continental margins and adjacent seas, that frequently form the origin of our sediment-based data sets. We thus obtained a comparison of our empiric values with model estimates of

Muglia et al. (2018; 0–50 m w.d.; Fig. 8c-d; Table 3) only. Their model includes ocean surface reservoir age and ocean radiocarbon fields that have been validated through a comparison to LGM ^{14}C data compilation made by Skinner et al. 2017. It conforms two plausible, recent model estimates of surface reservoir ages that can be compared to our results (Table 3).

Low LGM values (300–750 yr) supposedly document an intensive exchange of surface waters with atmospheric CO_2, most common in model- and foraminifera-based estimates of the low- and mid-latitude Atlantic. Low empiric values also mark LGM waters in mid to high latitudes off Norway and off middle Chile, that is, close to sites of potential deep and/or intermediate water formation. Off Norway and in the northeastern Atlantic, model-based reservoir ages of Muglia et al. (2018) largely match the empiric range. However, the uncertainty envelopes for data shown in Fig. 8c (±560 yr; r = 0.59) generally exceed by far the spatial differences calculated for the empiric data. Conversely, model-based reservoir ages reproduce only poorly the low planktic foraminifera-based estimates off Central Chile and values in the Western Pacific and Southern Ocean.

In part, the differences may be linked to problems like insufficient spatial resolution along continental margins, ignoring east-west differences within ocean basins, and/or the estimates of a correct location and extent of seasonal sea ice cover used as LGM boundary condition such as east off Greenland, in the subpolar northwest Pacific, and off Southern Chile, where sea ice hindered the exchange of atmospheric carbon (per analogy to that of temperature exchange, e.g., Sessford et al, 2019). Also, model estimates of the annual average are compared to ^{14}C signals of planktic foraminifera that mostly formed during summer only, e.g., when large parts of the Nordic Seas were found ice-free (Sarnthein et al., 2003). Hence, models may need to better constrain local and seasonal sealing effects of LGM sea ice cover.

In general, the foraminifera-based reservoir age estimates for our sites that represent various hydrographic key regions in the high-latitude ocean appear much higher than model-derived values. These deviations reach up to 1400 yr, in particular in the Southern Ocean. In part, they may result from the fact that present models may not yet be suited to capture small-scale ocean structures such as the interference of ocean currents with local bathymetry and local upwelling cells. Here, model-based reservoir ages appear far too low in LGM regions influenced by regional upwelling such as the South China Sea then governed by an estuarine overturning system (Wang et al., 2005; Fig. 9), by coastal upwelling off N.W. Australia (Xu et al., 2010; Sarnthein et al., 2011), or by a melt water lid such as off eastern New Zealand (Bostock et al., 2013; Küssner et al., in prep.). Local oceanic features are likely to be missed in current resolution models. Our more narrow-spaced empiric data could help to refine the skill of models to capture past ^{14}C reservoir ages.

Various differences amongst plankton- and model-based reservoir ages may also result from differential seasonal habitats of the different planktic species analyzed that, in turn, may trace different surface and subsurface water currents. Distinct interspecies differences were found in Baja California that record differential, upwelling-controlled habitat conditions (Lindsay et al, 2015). In the northern Norwegian Sea interspecies differences amount up to 600 yr for the Preboreal ^{14}C plateau, 9.6–10.2 cal. ka (Sarnthein and Werner, 2018). Here ^{14}C records of Arctic *Turborotalita quinqueloba*, dominantly grown close to the sea surface during peak summer, differ from the paired record of *Neogloboquadrina pachyderma*, formed in subsurface waters, and that of subpolar species *N. incompta*, mainly advected from the south by Norwegian Current waters well mixed with the atmosphere during peak winter. This makes closer specification of model results as product of different seasonal extremes a further target.

3.3 Planktic foraminifera-based ^{14}C reservoir ages – A prime database to estimate past changes in the ^{14}C ventilation age of deep waters and past oceanic MOC and DIC

'Raw' apparent benthic ventilation ages (in ^{14}C yr; 'raw' *sensu* Balmer et al., 2018) express the difference between the (coeval) atmospheric and benthic ^{14}C levels measured at any site and time of foraminifer deposition. These ages are the sum of (1) the planktic reservoir age of the ^{14}C plateau that covers a group of paired benthic and planktic ^{14}C ages and (2) the (positive or negative) ^{14}C age difference between any benthic ^{14}C age and the average ^{14}C age of the paired planktic ^{14}C plateau. The benthic ventilation ages necessarily rely on the high quality of ^{14}C plateau-based chronology, since the atmospheric ^{14}C level has been subject to substantial short-term changes over glacial-to-deglacial times. Necessarily, the ventilation ages include a mixing of different water masses that might originate from different ocean regions and may contribute differential ^{14}C ventilation ages, an unknown justifying the modifier 'apparent'.

In a further step, the $\Delta\Delta^{14}$C equivalent of our 'raw' benthic ventilation age may be adjusted to changes in atmospheric ^{14}C that occurred over the (short) time span between deep-water formation and benthic sediment deposition (e.g., Balmer and Sarnthein, 2018; Cook and Keigwin, 2015). In most cases, however, this second step is omitted since its application usually does not imply any major modification of the ventilation age estimates (Fig. S2a; Skinner et al., 2017; Sarnthein et al., 2013).

On the basis of ^{14}C plateau tuning we now can rely on 18 accurately dated records of apparent benthic ^{14}C ventilation ages (Fig. S2a-d) to reconstruct the global geometry of LGM and HS-1 deep and intermediate water circulation as summarized in ocean transects and maps (Figs. 9–11) and discussed below. The individual matching of our 20 planktic ^{14}C plateau sequences with that of the Suigetsu atmospheric ^{14}C record is displayed in Sarnthein et al. (2015), Balmer et al., (2016), Küssner et al. (in prep.), and Ausin et al. (in prep.). In addition, robust estimates of past reservoir ages are obtained for 4 planktic and benthic ^{14}C records from paired atmospheric ^{14}C ages of wood chunks (Rafter et al., 2018; Zhao and Keigwin, 2018; Broecker et al., 2004).

3.3.1 — Major features of ocean meridional overturning circulation during LGM (Fig. 10)

Off Norway and near the Azores Islands very low benthic ^{14}C ventilation ages of <100–750 yr suggest ongoing deep-water formation in the LGM northern North Atlantic reaching down to more than 3000–3500 m water depth, with a flow strength possibly similar to today (and a coeval deep countercurrent of old waters from the Southern Ocean flowing along the East Atlantic continental margin off Portugal). This pattern clearly corroborates the assembled benthic $\delta^{13}C$ record showing plenty of elevated $\delta^{13}C$ values for the northwestern, eastern and central North Atlantic (Sarnthein et al., 1994; Millo et al., 2006; Keigwin and Swift, 2017). Irrespective of unspecified potential zonal variations in deep-water ventilation age at mid latitudes and different from a number of published models (e.g., Ferrari et al., 2014; Butzin et al., 2017) this 'anti-estuarine' pattern has been confirmed by MIROC model simulations (Gebbie, 2014; Sherriff-Tadano et al., 2017, Yamamoto et al., 2019) and, independently, by ε_{Nd} records (Howe et al., 2016; Lippold et al., 2016). The latter suggest an overturning of AMOC possibly even stronger than today, in particular due to a 'thermal threshold' (Abé-Ouchi, pers. comm.) overlooked in other model simulations.

In contrast to the northern North Atlantic, deep waters in the southern North Atlantic and Circumpolar (CP) deep waters in the subpolar South Atlantic show an LGM ^{14}C ventilation age of ~3640 yr, finally rising up to 3800 yr (Figs. 10, 11, S2b). These waters were upwelled and admixed from below to surface waters near to the sub-Antarctic Front during terminal LGM (Fig. S2b; Skinner et al., 2010; Balmer and Sarnthein, 2016; model of Butzin et al., 2012).

In the southwestern South Pacific abyssal, in part possibly Antarctic-sourced waters (Rae and Broecker, 2018) likewise show high apparent ^{14}C ventilation ages that vary from 3800 to 4300 yr over the LGM (Figs. 10 top and S2c) (^{14}C dates of Ronge et al., 2016, modified by planktic ^{14}C reservoir ages of Küssner et al., in prep.). A vertical transect of benthic $\delta^{13}C$ (McCave et al., 2008) suggests that the abyssal waters were overlain by CP waters, separated by pronounced stratification near ~3500–4000 m water depth. In part, the CP waters stemmed from North Atlantic Deep Water. Probably, their apparent ventilation age 3800–4300 yr came close to the values found in the southern South Atlantic. East of New Zealand the CP waters entered the deep western Pacific and spread up to the subpolar North Pacific, where LGM ^{14}C ventilation ages reached ~3700 yr, possibly occasionally 5000 yr (Fig. S2d).

Similar to today, the MOC of the LGM Pacific was shaped by estuarine geometry, probably more weakened than today (Du et al., 2018) and more distinct in the far northwest than in the far northeast. This geometry resulted in an upwelling of old deep waters in the subarctic Northwest Pacific, here leading to a ^{14}C reservoir age of ~1700 yr for surface waters at terminal LGM. On top of the Lower Pacific Deep Waters we may surmise Upper Pacific Deep Waters that moved toward south (Figs. 10 top and 11).

The Pacific deep waters were overlain by Antarctic / Pacific Intermediate Waters (IW) with LGM ^{14}C ventilation ages as low as 1400–1600 yr, except for a shelf ice-covered site at the southern tip of Chile with IW ages of 1400–2900 yr, possibly a result of local upwelling of CP waters. In general, however, the low values of Pacific IW are similar to those estimated for South Atlantic IW and likewise reflect a vivid exchange with atmospheric CO_2 in their source regions in the Southern Ocean (Skinner et al., 2015).

When entering and crossing the entrance sill to the marginal South China Sea the ‘young’ IW were mixed with ‘old’ CP waters entrained from below, here leading to ^{14}C ventilation ages of 2600–3450 yr (Figs. 9 and S2d). The LGM South China Sea was shaped by an estuarine-style overturning system marked by major upwelling near to its distal end in the far southwest (Wang L. et al., 1999). This upwelling led to planktic ^{14}C reservoir ages as high as 1200–1800 yr, values rarely found elsewhere in surface waters of low latitudes.

Our wide-spaced distribution pattern of 18 open-ocean ^{14}C ventilation ages (plus 4 values based on paired wood chunks) in Figs. 10 and 11 agrees only in part with the circulation patterns suggested by the much larger datasets of ^{14}C ventilation ages compiled by Skinner et al. (2017) and Zhao et al. (2018). Several features in Figs. 10 and 11 directly deviate, e.g., the ages we derive for the North Atlantic and mid-depth Pacific. These deviations may be linked to both the different derivation of our ^{14}C ventilation age estimates and the details of our calendar-year chronology now based on the narrow-standing suite of ^{14}C plateau-boundary ages. The quality of our ^{14}C reservoir ages of surface waters also controls the 'apparent' ventilation age of deep-waters, as it results from direct addition of the short-term average ^{14}C age of a planktic ^{14}C plateau to a paired, that is coeval benthic ^{14}C age (formed during the time of benthic foraminiferal growth, somewhat after the actual time of deep-water formation).

3.3.2 — Major features of meridional overturning circulation during early HS-1 (Fig. 10)

Near the onset of deglacial Heinrich Stadial 1 (HS-1; ~18–14.7 cal. ka) major shifts in ^{14}C ventilation age suggest some short-lasting but fundamental changes in the circulation geometry of the deep ocean, a central theme of marine paleoclimate research (lower panel of Figs. 10, 11 and S2a and b). Deep waters in the eastern Nordic Seas, west of the Azores Islands, and off northern Brazil show a rapid rise to high ^{14}C ventilation ages of ~2000–2500 yr and up to 4000 yr off Brazil, values that give first proof for a brief switch from ‘anti-estuarine’ to ‘estuarine’ circulation that governed the central North Atlantic and Norwegian Sea during early HS-1. This geometry continued – except for a brief but marked and widespread event of recurring NADW formation near 15.2 ka – until the very end of HS-1 near 14.5 ka (Fig. S2a; Muschitiello et al., 2019). The MOC switch from LGM to HS-1 is in line with changes depicted in paired benthic $\delta^{13}C$ data (Sarnthein et al., 1994), but not confirmed by the coeval ε_{Nd}

record that suggests a constant source of ‘mid-depth waters’, with the $\delta^{13}C$ drop being simply linked to a higher age (Howe et al., 2018).

Conversely, benthic ^{14}C ventilation ages in the northeastern North Pacific (Site MD02-2489) show a coeval and distinct but brief minimum of 1050-1450 yr near 3640 m w.d. during early HS-1 (~18.1–16.8 ka; Figs. 10, 11, and S2d). This minimum was produced by extremely small benthic-planktic age differences of 350–650 yr and provides robust evidence for a millennial-scale event of deep-water formation, that has flushed the northeastern North Pacific down to more than 3640 m w.d. (Gebhardt et al., 2008; Sarnthein et al., 2013; Rae et al., 2014). Similar circulation geometries were reported for the Pliocene (Burls et al., 2017). ‘Young’ Upper North Pacific Deep Waters (North Pacific Intermediate Waters *sensu* Gong et al., 2019) then penetrated as ‘western boundary current’ far south, up to the northern continental margin of the South China Sea (Figs. 9b, 11, and S2d). The short-lasting North Pacific regime of anti-estuarine overturning was similar to that we find in the modern and LGM Atlantic and, most interesting, simultaneous with the Atlantic's estuarine episode.

Recent data on benthic-planktic ^{14}C age differences (Du et al., 2018) precisely recover our results in a core at ~680 m w.d. off southern Alaska. However, they do not depict the ‘young’ deep waters at their Site U1418 at ~3680 m w.d., as corroborated by a paired autigenic ε_{Nd} maximum suggesting a high local bottom water age nearby. We assume that the amazing difference in local deep-water ventilation ages is due to small-scale differences in the effect of Coriolis forcing at high latitudes between a site located directly at the base of the Alaskan continental margin (U1418; Fig. 10b) and that on the distal Murray Sea Mount in the ‘open’ Pacific (MD02-2489; Figs. 7 and 11), which probably has been been washed by a plume of newly formed North Pacific deep waters probably stemming from the Bering and/or Ochotsk Seas. In contrast, the incursion of almost 3000 yr old deep waters from the Southern Ocean has continued along the continental margin all over HS-1. In summary we may conclude that the geometry of ocean MOC was briefly reversed in the 'open' North Pacific over almost 1500 years during HS-1, far deeper than suggested by previous authors (e.g., Okazaki et al., 2012; Gong, S., et al. 2019), but similar to changes in geometry first proposed by Broecker et al. (1985) then, however, for an LGM ocean.

3.3.3 — Deep-Ocean DIC inventory

Apart from the changing geometries in ocean MOC during LGM and HS-1, the global set of ^{14}C plateau-based, hence refined estimates of apparent ^{14}C ventilation ages (Fig. 10) has ultimately also revealed new insights into glacial-to-deglacial changes in deep-ocean DIC inventories (Sarnthein et al., 2013; Skinner et al., 2019). On the basis of GLODAP data (Key et al., 2004) any drop in ^{14}C concentration (i.e., any rise in average ^{14}C ventilation age) of modern deep waters is tied linearly to a rise of carbon (DIC) dissolved in deep ocean waters below ~2000 m, making for 1.22 micromole C / -1 ‰ ^{14}C. By and large, GCM and box model simulations of Chikamoto and Abé-Ouchi (2012) and Wallmann et al. (2016) suggest that this ratio may also apply to LGM deep-water circulation, when apparent ^{14}C ventilation ages in the Southern Ocean increased significantly (from 2400 up to ~5000 yr) and accordingly, thermohaline circulation was more sluggish and transit times of deep waters extended. Accordingly, a 'back-of-the-envelope' calculation of LGM ventilation age averages in the global deep ocean suggests an additional carbon absorption of 730–980 Gt (Sarnthein et al., 2013). This estimate can easily accommodate the glacial transfer of ~200 Gt C from the atmosphere and biosphere, moreover, may also explain 200–450 Gt C then most probably removed from glacial Atlantic and Pacific intermediate waters. These estimates offer an independent evaluation of ice core-based data, other proxies, and model-based data on past changes in the global carbon cycle (e.g., Menviel et al., 2018).

4. SOME CONCLUSIONS AND PERSPECTIVES

– Despite some analytical scatter, ^{14}C ages for the top and base of Lake Suigetsu-based atmospheric ^{14}C plateaus and coeval planktic ^{14}C plateaus do not present statistical 'outliers' but real age estimates that are reproduced by tree ring-based ^{14}C ages over the interval 10–13 cal. ka and further back.

– Hulu U/Th model-based ages of ^{14}C plateau boundaries of the Suigetsu atmospheric ^{14}C record appear superior to those derived from microscopy-based varve counts only, since U/Th model-based ages match far more closely the age when now deduced from XRF-based varve counts for the tie point of lower plateau boundary 2b, a test case in the early deglacial, and for the age assigned to the Laschamp event prior to the LGM.

– During deglacial times, we show that several atmospheric ^{14}C plateaus paralleled a rise in air-sea gas exchange, and, in turn, distinct changes in ocean MOC. Changes in cosmogenic ^{14}C production rarely provide a complete explanation for the plateaus identified in the Suigetsu ^{14}C data under discussion.

– In total, ^{14}C plateau boundaries in the range now provide a suite of ~30 age tie points to establish – like chronological ladder rungs – a robust global age control for deep-sea sediment sections and global stratigraphic correlations of last glacial to deglacial climate events, 29–10 cal. ka. U/Th model ages confine the cal. age uncertainty of Suigetsu plateau boundaries assigned halfway between two ^{14}C ages nearby inside and outside a plateau's scatter band to less than ±50 to ±70 yr. Nevertheless, stratigraphic gaps may hamper the accurate tuning of planktic ^{14}C plateaus to their atmospheric equivalents hence result in major discrepancies.

– The difference in ^{14}C age between coeval atmospheric and planktic ^{14}C plateaus presents a robust tracer of planktic ^{14}C reservoir ages and shows their high temporal and spatial variability for the LGM and HS-1, now established for 18/20 sediment sites.

– Paired reservoir ages obtained from different planktic species document the local distribution patterns of different surface water masses and prevailing foraminiferal habitats at different seasons yet insufficiently considered in model simulations.

– New, more robust deep-water ^{14}C ventilation ages, derived on the basis of our robust planktic ^{14}C reservoir ages, reveal geometries of LGM overturning circulation similar to those of today. In contrast, ^{14}C ventilation ages of early HS-1 suggest an almost 1500 yr long event of widely reversed circulation patterns marked by deep-water formation and brief flushing of the northern North Pacific and estuarine circulation geometry in the northern North Atlantic.

– Increased glacial ^{14}C ventilation ages and carbon (DIC) inventories of ocean deep waters suggest an LGM drawdown of about 850 Gt C into the deep ocean. Starting with HS-1 a drop of ventilation age suggests carbon released to the atmosphere (Sarnthein et al., 2013).

– Site-specific comparison of planktic and model-based reservoir ages estimates highlights the need for further model refinements to make them better reflect the real complex patterns of ocean circulation, including seasonality.

ACKNOWLEDGMENTS

We owe sincere thanks for plenty of stimulations to the 23rd International Radiocarbon Conference in Trondheim, in particular to M-J. Nadeau, and to the IPODS–OC3 workshop in Cambridge U.K, 2018, convened by A. Schmittner and L. Skinner. Moreover, we thank for most valuable basic discussions with R. Staff, Glasgow, J. Southon, Irvine CA, and M. Butzin, AWI Bremerhaven, who kindly helped us to discuss the comparison of his model results, and S. Beil, Kiel, for computer assistance. Over the last three years, G. Mollenhauer measured with care hundreds of supplementary ^{14}C ages in her MICADAS laboratory at AWI Bremerhaven. This study obtained long lasting special support from R. Tiedemann and his colleagues at the AWI Bremerhaven.

Author contribution

All authors contributed data and valuable suggestions to write up this synthesis. MS and PG designed the outline of this manuscript. KK, BA, TE and MS provided new marine ^{14}C records in addition to records previously published. GS displayed the details of Suigetsu varve counts. RM provided a ^{10}Be-based ^{14}C record and plots of raw ^{14}C data sets of Suigetsu und Hulu Cave. Discussions amongst PG, RM, GS and MS served to select U/Th-based model ages as best-possible time scale. JM streamlined the sections on data-model intercomparison.

Data availability

Published primary radiocarbon data of most sites are available at PANGAEA de. ^{14}C data of 5 marine cores still under publication by Küssner et al. (in prep.) and Ausin et al. (in prep.; also see caption of Fig. S2) are deposited at PANGAEA still under embargo.

REFERENCES (99)

Adkins, J. F. and Boyle, E. A.: Changing atmospheric $\Delta^{14}C$ and the record of paleoventilation ages. Paleoceanography, 12(3), 337–344, 1997.

Adolphi, F., Bronk Ramsey, C., Erhard, T., Lawrence Edwards, R., Cheng, H., Turney, C.S.M., Cooper, A., Svensson, A., Rasmussen, S.O., Fischer, H., and

Muscheler, R.: Connecting the Greenland ice-core and U/Th timescales via cosmogenic radionuclides: testing the synchroneity of Dansgaard–Oeschger events. Clim. Past, 14, 1755–1781. https://doi.org/10.5194/cp-14-1755-2018, 2018.

Alves, E.Q., Macario, K., Ascough, P., and Bronk Ramsey, C.: The worldwide marine radiocarbon reservoir effect: definitions, mechanisms, and prospects. Review of Geophysics, 56, https://doi.org/10.1002/2017RG000588, 2018.

Alveson, E.Q.: Radiocarbon in the Ocean, EOS, 99, https://doi.org/10.1029/2018EO095429, 2018.

Ausin, B., Haghipour, N., Wacker, L., Voelker, A. H. L., Hodell, D., Magill, C., et al.: Radiocarbon age offsets between two surface dwelling planktonic foraminifera species during abrupt climate events in the SW Iberian margin. Paleoceanography and Paleoclimatology, 34. https://doi.org/10.1029/2018PA003490, 2019.

Balmer, S., Sarnthein, M., Mudelsee, M., and Grootes, P. M.: Refined modeling and ^{14}C plateau tuning reveal consistent patterns of glacial and deglacial ^{14}C reservoir ages of surface waters in low-latitude Atlantic. Paleoceanography, 31. https://doi.org/10.1002/2016PA002953, 2016.

Balmer, S. and Sarnthein, M.: Planktic ^{14}C plateaus, a result of short-term sedimentation pulses? – Radiocarbon, 58, DOI:10.1017/RDC.2016.100, 11 pp., 2016.

Balmer, S. and Sarnthein, M.: Glacial-to deglacial changes in North Atlantic melt-water advection and deep-water formation – Centennial-to-millennial-scale ^{14}C records from the Azores Plateau. Geochim. Cosmochim. Acta, 236, 399-415, https://doi.org/10.1016/j.gca.2018.03.001, 2018.

Berger W.H. and Keir, R.S.: Glacial-Holocene changes in atmospheric CO_2 and the deep-sea record. J.E. Hansen, T. Takahashi (Eds.), Geophysical Monograph, 29, American Geophysical Union, Washington, DC, pp. 337–351, 1984.

Bostock, H.C., Barrows, T.T., Carter, L., Chase, Z., Cortese, G., et al.: A review of the Australian – New Zealand sector of the Southern Ocean over the last 30 ka (Aus-INTIMATE project). Quaternary Science Reviews 74, 35-57, 2013.

Broecker W.S, Peteet, D.M., and Rind, D.: Does the ocean-atmosphere system have more than one stable mode of operation? Nature, **315**, 21-26, doi:10.1038/315021a0, 1985

Broecker W.S., Barker, S., Clark, E., Hajdas, I., Bonani, G., and Stott, L.: Ventilation of the Glacial deep Pacific Ocean, Science, 306, 1169–1172, 2004.

Bronk Ramsey, C., Staff, R. A., Bryant, C. L., Brock, F., Kitagawa, H., van der Plicht, J., Schlolaut, G., Marshall, M. H., Brauer, A., Lamb, H. F., Payne, R. L., Tarasov, P. E., Haraguchi, T., Gotanda, K., Yonenobu, H., Yokoyama, Y., Tada, R., and Nakagawa, T.: A complete terrestrial radiocarbon record for 11.2 to 52.8 kyr B.P., Science, 338, 370–374, 2012.

Bronk Ramsey, C. et al., Radiocarbon, (in press) 2020.

Burke, A. and Robinson, L.F.: The Southern Ocean's role in carbon exchange during the last deglaciation. Science, 335, 557-561, 2012.

Burls, N.J., Fedorov, A.V., Sigman, D.M., Jaccard, S.L., Tiedemann, R., and Haug, G.H.: Active Pacific meridional overturning circulation (PMOC) during the warm Pliocene. Sci. Adv. 2017;3: e1700156, 2017.

Butzin, M., Prange, M., Lohmann, G.: Radiocarbon simulations for the glacial ocean: The effects of wind stress, Southern Ocean sea ice and Heinrich events. Earth Planet. Sci. Lett., 235, 45-61, 2005.

Butzin, M., Prange, M., and Lohmann, G.: Readjustment of glacial radiocarbon chronologies by self-consistent three-dimensional ocean circulation modeling. Earth Planet Sci. Lett., 317, 177-184, 2012.

Butzin, M., Köhler, P., and Lohmann, G.: Marine radiocarbon reservoir age simulations for the past 50,000 years. Geophys. Res. Lett., 44, 8473–8480, doi:10.1002/2017GL074688, 2017.

Butzin, M., Heaton, T.J., Köhler, P., and Lohmann, G.: A short note on marine reservoir age simulations used in INTCAL20. Radiocarbon, oo, 1-7, DOI:10.1017/RDC.2020.9, 2020.

Chen, T., Robinson, L.F., Burke, A., Southon, J., Spooner, P., Morris, P.J., and Ng, H.C.: Synchronous centennial abrupt events in the ocean and atmosphere during the last deglaciation, Science, 349, 1537-1541, 2015.

Cheng, H., Edwards, R.L., Southon, J., Matsumoto, K., Feinberg, J.M., Sinha, A., Zhou, W., Li, H., Li, X., Xu, Y., Chen, S., Tan, M., Wang, Q., Wang, Y., and Ning, Y.: Atmospheric 14C/12C changes during the last glacial period from Hulu Cave, Science, 362, 1293-1297, 2018.

Chikamoto, M.O., Abé-Ouchi, A., Oka, A., Ohgaito, R., and Timmermann, A.: Quantifying the ocean's role in glacial CO_2 reductions, Climate of the Past, 8, 545–563, doi:10.5194/cp-8-545-2012, 2012.

Cook M.S. and Keigwin L.D.: Radiocarbon profiles of the NW Pacific from the LGM and deglaciation: Evaluating ventilation metrics and the effect of uncertain surface reservoir ages, Paleoceanography, 30, 174–195, 2015.

Davies, S.M., Davies, P.M., Abbott, Meara, R.H., et al.: A North Atlantic tephro-stratigraphical framework for 130-60 ka b2k: New tephra discoveries, marine based correlations, and future challenges, Quaternary Science Rev., 106, 101-121, 2014.

Du, J., Haley, B.A., Mix, A.C., Walczak, M.H., and Praetorius, S.K.: Flushing of the deep Pacific Ocean and the deglacial rise of atmospheric CO_2 concentrations, Nature geoscience, 11, 749-755, 2018.

Ferrari, R., Jansen, M.F., Adkins, J.F., Burke, A., Stewart, A.L., and Thompson, A.F.: Antarctic sea ice control on ocean circulation in present and glacial climates, Proc. National Academy Science, 111 (24), 8753–8758, 2014.

Gebbie, G.: How much did Glacial North Atlantic Water shoal? Paleoceanography, 29, 190-209, doi:10.1002/2013PA002557, 2014.

Gebhardt, H., Sarnthein, M., Kiefer, T., Erlenkeuser, H., Schmieder, F., and Röhl, U.: Paleonutrient and productivity records from the subarctic North Pacific for Pleistocene glacial terminations I to V. Paleoceanography 23, PA4212, 1-21, doi:10.1029/2007PA001513, 2008.

Gong, S., Lembke-Jene, L., Lohmann, G., Knorr, G., Tiedemann, R., Zou, J.J and Shi, X.F.: Enhanced North Pacific deep-ocean stratification by stronger intermediate water formation during Heinrich Stadial 1. Nature Communications, 10: 656. https://doi.org/10.1038/s41467-019-08606-2, 2019.

Grootes P.M. and Stuiver, M.: Oxygen 18/16 variability in Greenland snow and ice with 1000 to 100000 year time resolution, J. Geophys. Res.: Oceans (1978–2012) 102(C12), 26455–26470, 1997.

Grootes, P.M. and Sarnthein, M.: Marine ^{14}C reservoir ages oscillate, PAGES News, 14/3, 18-19, 2006.

Hain, M.P., Sigman, D.M., and Haug, G.H.: Distinct roles of the Southern Ocean and North Atlantic in the deglacial atmospheric radiocarbon decline, Earth Planetary Science Letters 394, 198-208, 2014.

Howe, J.N.W., Piotrowski, A.M., Noble, T.L., Mulitza, S., Chiessi, C.M., and Bayon, G.: North Atlantic deep-water production during the last glacial maximum, Nat. Commun., 7, 11765, 2016. s

Howe, J.N.W., Huang, K-F., Oppo, D.W., Chiessi, C.M., Mulitza, S., Blusztajn, J., and Piotrowski, A.M.: Similar mid-depth Atlantic water mass provenance during the Last Glacial Maximum and Heinrich Stadial 1, Earth Planetary Science Letters, 490, 51-61, 2018.

Jonkers, L. and Kucera, M.: Quantifying the effect of seasonal and vertical habitat tracking on planktonic foraminifera proxies, Climate of the Past, 13, 573-586, 2017.

Keigwin, L.D. and Swift, S.A.: Carbon isotope evidence for a northern source of deep water in the glacial western North Atlantic, PNAS, 114 (11), 2831-2835, 2017.

Key R. M., Kozyr, A., Sabine, C.L., Lee, K., Wanninkhof, R., Bullister, J.L., Feely, R.A., Millero, F.J., Mordy, C., and Peng, T.-H. (2004) A global ocean carbon climatology: Results from Global Data Analysis Project (GLODAP), Global Biogeochem. Cy., 18, GB4031, doi:10.1029/2004GB002247, 2004.

Kong, X., Wang, Y., Wu, J., Cheng, H., Edwards, R.L., and Wang, X.: Complicated responses of stalagmite $\delta^{13}C$ to climate change during the last glaciation from Hulu Cave, Nanjing, China, Science in China Ser. D Earth Sciences, 48, (12), 2174-2181, 2005.

Küssner, K., Sarnthein, M., Lamy, F., and Tiedemann, R.: High-resolution radiocarbon-based age records trace episodes of *Zoophycos* burrowing, Marine Geology, 403, 48-56, http://doi:10.1016/j.margeo.2018.04.01, 2018.

Küssner, K., Sarnthein, M., Lamy, F., Michel, E., Mollenhauer, G., Siani G., and Tiedemann, R.: Glacial-to-deglacial reservoir ages of surface waters in the southern South Pacific, Paleoc. and Paleoclim. 30 ms-pp, in prep.).

Lascu, I., Feinberg, J.M., Dorale, J.A., Cheng, H., and Edwards, R.L.: Age of the Laschamp excursion determined by U-Th dating of a spelothem geomagnetic record from North America. Geology, 44, 139-142, doi:10.1130/G37490.1. 2016

Lindsay, C.M., Lehman, S.J., Marchitto, T.M., and Ortiz, J.D.: The surface expression of radiocarbon anomalies near Baja California during deglaciation. Earth Planetary Science Letters, 422, 67-74, 2015.

Lippold, J., Gutjahr, M., Blaser, P., Christner, E., de Cavalho-Fereira, M.L., Mulitza, S. et al.: Deep-water provenance and dynamics of the (de)glacial Atlantic meridional overturning circulation, Earth Planetary Science Letters, 445, 68-78, 2016.

Lisiecki, L.E. and Stern, J.V.: Regional and global benthic $d^{18}O$ stacks for the last glacial cycle. Paleoceanography, 31, doi:10.1002/2016PA003002, 2016.

Löwemark, L. and Grootes, P.M.: Large age differences between planktic foraminifers caused by abundance variations and Zoophycos bioturbation, Paleoceanography, 19, PA2001, doi:10.1029/2003PA000949, 2004.

Marcott, S.A., Bauska, T.K., Buizert, C., Steig, E.J., Rosen, J.L., Cuffey, K.M., Fudge, T.J., Severinghaus, J.P., Ahn, J., Kalk, M.L., McConnell, J.R., Sowers, T., Taylor, K.C., White, J.W.C., and Brook, E.J.: Centennial-scale changes in the global carbon cycle during the last deglaciation, Nature, 514, 616-619, doi:10.1038/nature13799, 2014.

Marshall, M., Schlolaut, G., Brauer, A., Nakagawa, T., Staff, R.A., Bronk Ramsey, C., Lamb, H., Gotanda, K., Haraguchi, T., Yokoyama, Y., Yonenobu, H., Tada, R., SG06 project members: A novel approach to varve counting using µXRF and X-radiography in combination with thin-section microscopy, applied to the Late Glacial chronology from Lake Suigetsu, Japan, Quaternary Geochronology 13, 70-80, 2012.

McCave, I.N., Carter, I., and Hall, I.R.: Glacial-interglacial changes in water mass structure and flow in the SW Pacific Ocean, Quaternary Science Rev., 27, 1886–1908, 2008.

Matsumoto, K.: Radiocarbon-based circulation age of the world oceans, J. Geophys. Res.: Oceans 112(C9), C09004. https://doi.org/10.1029/2007JC004095, 2007.

Menviel, L., Spence, P., Yu, J., Chamberlain, M.A., Matear, R.J., Meissner K.J., and England, M.H.: Southern Hemisphere westerlies as a driver of the early deglacial atmospheric CO2 rise, Nature communications, 9:2503, DOI:10.1038/s41467-018-04876-4, 2018.

Millo, C., Sarnthein, M., and Erlenkeuser, M.: Variability of the Denmark Strait Overflow during the Last Glacial Maximum, Boreas, 35, 50-60, 2006.

Muglia, J., Skinner, L., and Schmittner, A.: Weak overturning circulation and high Southern Ocean nutrient utilization maximized glacial ocean carbon, Earth and Planetary Science Letters 496, 47-56, 2018.

Muschitiello, F., D'Andrea, W.J., Schmittner, A., Heaton, T.J., Balascio, N.L., deRoberts, N., Caffee, M.W., Woodruff, T.E., Welten, K.C., Skinner, L.C., Simon, M.H., and Dokken T.M.: Deep-water circulation changes lead North Atlantic climate during deglaciation, Nature Communications 10, 1272, doi.org/10.1038/s41467-019-09237-3, 2019.

Naughton, F., Costas, S., Gomes, S.D., Desprat, S., Rodrigues, T., Sanchez Goñi, M.F., Renssen, H., Trigo, R., Bronk-Ramsey, C., Oliveira, D., Salgueiro, E., Voelker, A.H.L., and Abrantes, F.: Coupled ocean and atmospheric changes during Greenland stadial 1 in southwestern Europe, Quaternary Science Reviews, 212, 108-120, 2019.

Nydal R., Lovseth K., and Skogseth F. H.: Transfer of bomb ^{14}C to the ocean surface, Radiocarbon 22(3), 626–635, 1980.

Okazaki, Y., Sagawa, T., Asahi, H., Horikawa, K., and Onodera, J.: Ventilation changes in the western North Pacific since the last glacial period, Climate of the Past, 8, 17-24, doi:10.5194/cp-8-17-2012, 2012.

Paillard, D., Labeyrie, L., and Yiou, P.: Macintosh program performs time-series analysis, *Eos Trans, AGU,* **77**: 379, 1996.

Rae, JW.B. and W. Broecker, W.: What fraction of the Pacific and Indian oceans' deep water is formed in the Southern Ocean? Biogeosciences, 15, 3779-3794, 2018.

Rae, J., Sarnthein, M., Foster, G., Ridgwell, A., Grootes, P.M., and Elliott T.: Deep water formation in the North Pacific and deglacial CO_2 rise, Paleoceanography, 29, doi:10.1002/2013PA002570, 645–667, 2014.

Rafter, P.A., Herguera, J.-C., and Southon, J.R.: Extreme lowering of deglacial seawater radiocarbon recorded by both epifaunal and infaunal benthic foraminifera in a wood-dated sediment core, Climate of the Past 14, 1977–1989, 2018.

Reimer P.J., Bard, E., Bayliss, A., Beck, J. W., Blackwell, P.G., Bronk Ramsey, C., Buck, C.E., Cheng, H., Edwards, R.L., and Friedrich, M.: IntCal13 and Marine13 radiocarbon age calibration curves 0–50,000 years cal. BP, Radiocarbon 55, 1869–1887, 2013.

Reimer, P.J., et al.: The IntCal 20 northern hemisphere radiocarbon calibration curve (0-55 kcal BP), Radiocarbon, 2020 (in press).

Robinson, L.F., Adkins, J.F., Keigwin, L.D., et al..: Radiocarbon variability in the western North Atlantic during the last deglaciation, Science, 310, 1469-1473, 2005.

Ronge, T. A., Tiedemann, R., Lamy, F., et al.: Radiocarbon constraints on the extent and evolution of the South Pacific glacial carbon pool, Nature Comm. 7:11487, 2016.

Ronge, T.A., Sarnthein, M., Roberts, J., Lamy, F., and Tiedemann, R.: East Pacific Core PS75/059-2: Glacial-to-deglacial stratigraphy revisited, Paleoceanography and Paleoclimatology, 34 (4), 432-435, DOI:10.1029/2019PA003569, 2019.

Sarnthein, M., Winn, K., Jung, S.J., Duplessy, J.C., Labeyrie, L., Erlenkeuser, H., and Ganssen, G.: Changes in east Atlantic deepwater circulation over the last 30,000 years: eight time slice reconstructions, Paleoceanography, 9(2), 209–267, 1994.

Sarnthein, M., Pflaumann, U., and Weinelt, M.: Past extent of sea ice in the northern North Atlantic inferred from foraminiferal paleotemperature estimates, Paleoceanography, 18(2), 2003.

Sarnthein, M., Grootes, P.M., Kennett, J.P., and Nadeau, M.: ^{14}C Reservoir ages show deglacial changes in ocean currents and carbon cycle, Geophys. Monograph –

Am. Geophys. Union, 173, 175–196, 2007.

Sarnthein, M., Grootes, P.M., Holbourn, A., Kuhnt, W., and Kühn, H.: Tropical warming in the Timor Sea led deglacial Antarctic warming and almost coeval atmospheric CO_2 rise by >500 yr, Earth Planetary Science Letters, 302, 337-348, 2011.

Sarnthein, M., Schneider, B., and Grootes, P.M.: Peak glacial 14C ventilation ages suggest major draw-down of carbon into the abyssal ocean, Climate of the Past, 9 (1), 925–965, 2013.

Sarnthein, M., Balmer, S., Grootes, P.M., and Mudelsee, M.: Planktic and benthic 14C reservoir ages for three ocean basins, calibrated by a suite of 14C plateaus in the glacial-to-deglacial Suigetsu atmospheric 14C record, Radiocarbon, 57, 129–151, 2015.

Sarnthein, M. and Werner, K.: Early Holocene planktic foraminifers record species-specific ^{14}C reservoir ages in Arctic Gateway, Marine Micropaleontology, 135, 45-55. DOI:10.1016/j.marmicro.2017.07.002, 2018.

Schlolaut, G.: A unique and easy-to-use-tool to deal with incompletely varved archives 782 – the Varve Interpolation Program 3.0.0, Quaternary Geochronology, 2019 (in press).

Schlolaut, G., Staff, R.A., Marshall, M.H., Brauer, A., Bronk Ramsey, C., Lamb, H.F., and Nakagawa, T.: Microfacies analysis of the Lake Suigetsu (Japan) sediments from ~50 to ~10 ka BP and an extended and revised varve based chronology, Quaternary Science Reviews, 200, 351-366, 2018.

Schmittner, A. and Lund, D.C.: Early deglacial Atlantic overturning decline and its role in atmospheric CO_2 rise inferred from carbon isotopes (δ^{13}C), Climate of the Past, 11, 135-152, 2015.

Schroeder, J., Holbourn, A., Küssner, K., and Kuhnt, W.: Hydrological variability in the southern Makassar Strait during the last glacial termination, Quaternary Science Reviews, 154, 143-156, 2016.

Sessford, E.G., Jensen, M.F., Tisserand, A.A., Muschitiello, F., Dokken, T., Nisancioglu, K.H., and Jansen, E.: Consistent fluctuations on intermediate water temperature off the coast off Greenland and Norway suring Dansgaard-Oeschger events, Quaternary Science Reviews, 223, 105887, 1-17, 2019.

Sherriff-Tadano, S., Abe-Ouchi, A., Yoshimori, M., Oka, A., and Chan, W.-L.: (Influence of glacial ice sheets on the Atlantic meridional overturning circulation through surface wind change, Climate Dynamics, 50 (7-8), 2881–2903, 2017.

Siani, G., Michel, E., De Pol-Holz, R., DeVries, T., Lamy, F., Carel, M., Isguder, G., Dewilde, F., Lourantou, A.: Carbon isotope records reveal precise timing of enhanced Southern Ocean upwelling during the last deglaciation, Nature Communications, 4, 2758, 2013.

Sikes, E.L. and Guilderson, T.P.: Southwest Pacific Ocean surface reservoir ages since the last deglaciation: Circulation insights from multiple-core studies. Paleoceanography, 31, 298–310, doi:10.1002/2015PA002855, 2016.

Simstich, J., Sarnthein, M., and Erlenkeuser, H.: Paired $\delta^{18}O$ signals of *Neogloboquadrina pachyderma* (s) and *Turborotalita quinqueloba* show thermal stratification structure in Nordic Seas, Mar. Micropaleontol., 912, 1–19, 2003.

Skinner, L.C., Fallon, S., Waelbroeck, C., Michel, E., and Barker, S.: Ventilation of the deep Southern Ocean and deglacial CO2 rise, Science, 328, 1147–1151, 2010.

Skinner, L.C., Waelbroeck, C., Scrivner, A.E., and Fallon, S.J.: Radiocarbon evidence for alternating northern and southern sources of ventilation of the deep Atlantic carbon pool during the last deglaciation, PNAS, 111, 5480–5484, 2014.

Skinner, L.C. *et al.*: Reduced ventilation and enhanced magnitude of the deep Pacific carbon pool during the last glacial period, Earth Planetary Science Letters, **411**, 45-52, 2015.

Skinner, L.C., Primeau, F., Freeman, E., de la Fuente, M., Goodwin, P.A., Gottschalk, J., Huang, E., McCave, I.N., Noble, T.L., and Scrivner A.E.: Radiocarbon constraints on the glacial ocean circulation and its impact on atmospheric CO_2, Nature communications, 8:16010, DOI: 10.1038/ncomms16010, 2017.

Skinner, L.C., Muschitiello, F., and Scrivner, A.E.: Marine reservoir age variability over the last deglaciation: Implications for marine carbon cycling and prospects for regional radiocarbon calibrations. Paleoceanography and Paleoclimate, 34, doi.org/10.1029/2019PA003667, 2019.

Southon, J., Noronha, A.L., Cheng, H, Edwards, R.L., and Wang, Y.: A high-resolution record of atmospheric ^{14}C based on Hulu Cave speleothem H82, Quaternary Science Reviews, 33:32-41, 2012.

Steffensen, J.P., Andersen, K.K., Bigler, M., et al.: High-Resolution Greenland Ice Core Data Show Abrupt Climate Change Happens in Few Years, Science, 321, 680; DOI: 10.1126/science.1157707, 2008.

Stern, J.V. and Lisiecki, L.E.: North Atlantic circulaton and reservoir age changes over the past 41,000 years, Geophysical Research Letters, 40, 3693-3697, doi:10.1002/grl.5067, 2013.

Stocker, T. and Johnsen, S.J.: A minimum thermodynamic model for the bipolar seesaw, Paleoceanography, 18 (4), 1087, doi:10.1029/2003PA000920, 2003.

Stuiver, M. and Braziunas, T.V.: Modeling atmospheric ^{14}C influences and ^{14}C ages of marine samples to 10,000 B.C., Radiocarbon, 35, 137–189, 1993.

Svensson, A., Andersen, K.K., Bigler, M., Clausen, H.B., Dahl-Jensen, D., Davies, S.M., Johnsen, S.J., Muscheler, R., Parrenin, F., Rasmussen, S.O., Röthlisberger, R., Seierstad, I., Steffensen, J.P., and Vinther, B.M.: A 60 000 year Greenland stratigraphic ice core chronology, Climate of the Past, 4, 47–57, 2008.

Toggweiler, J.R., Druffel, E.R.M., Key, R.M., and Galbraith, E.D.: Upwelling in the ocean basins north of the ACC. Part 2: How cool Subantarctic water reaches the surface in the tropics, J. Geophysical Research, DOI:10.1029/2018JC014795, 2019 (in press).

Turney, C.S.M., Fifield, L.K., Hogg, A.G., et al.: Using New Zealand kauri (*Agathis australis*) to test the synchronicity of abrupt climate change during the Last Glacial Interval (60,000–11,700 years ago), Quatern. Sci. Rev., 29, 3677–3682, 2010.

Turney, C.S.M., Jones, R.T., Phipps, S.J., et al.: Rapid global ocean-atmosphere response to Southern Ocean freshening during the last glacial, Nature communications, 8:520, doi:10.1038/s41467-017-00577-6, 2017.

Umling, N.E. and Thunnell, R.C.: Synchronous deglacial thermocline and deep-water ventilation in the eastern equatorial Pacific, Nature communications, 8, 14203. DOI: 10.1038/ncomms14203, 2017.

Waelbroeck, C., Duplessy, J.-C., Michel, E., Labeyrie, L., Paillard, D., and Duprat, J.: The timing of the last deglaciation in North Atlantic climate records, Nature, 412, 724–727, 2001.

Waelbroeck, C., Skinner, L.C., Labeyrie, L., Duplessy, J.-C., Michel, E., Riveiros, N.V., Gherardi, J.-M., and Dewilde, F.: The timing of deglacial circulation changes in the Atlantic, Paleoceanography, 26, PA3213, https://doi.org/10.1029/2010PA002007, 2011.

Wallmann, K., Schneider, B., and Sarnthein, M.: Effects of eustatic sea-level change, ocean dynamics, and nutrient utilization on atmospheric pCO_2 and seawater composition over the last 130,000 years – a model study, Climate of the Past, 12, 339-375, doi: 10.5194/cp-12-339-2016, 2016.

Wang Y.C, Cheng, H., Edwards, R.L., An, Z.S., Wu, J.Y., Shen, C.-C., and Dorale, J.A.: A high-resolution absolute-dated Late Pleistocene monsoon record from Hulu Cave, China, Science, 294, 2345-2348. DOI: 10.1126/science.1064618, 2001.

Wang, L.J., Sarnthein, M., Erlenkeuser, H., Grimalt, J., Grootes, P., Heilig, S., Ivanova, E., Kienast, M., Pelejero, C., and Pflaumann, U.: East Asian monsoon climate during the late Pleistocene: High-resolution sediment records from the South China Sea, Marine Geology, 156, 245-284, 1999.

Wang, P., Clemens, S., Beaufort, L., Braconnot, P., Ganssen, G., Jian, Z., Kershaw, P., and Sarnthein, M.: SCOR/IMAGES Working Group 113 SEAMONS: Evolution and variability of the Asian Monsoon System: State of the art and outstanding issues, Quaternary Science Reviews, 24 (5-6), 595-629, 2005.

WAIS Divide Project Members: Onset of deglacial warming in West Antarctica driven by local orbital forcing. Nature, 500, 440-444. doi:10.1038/nature12376, 2013.

Xu, J., Kuhnt, W., Holbourn, A., Regenberg, M., and Andersen, N.: Indo-Pacific Warm Pool variability during the Holocene and Last Glacial Maximum, Paleoceanogr., 25, 16, 2010.

Yamamoto, A., Abe-Ouchi, A., Ohgaito, R., Ito, A., and Oka, A.: Glacial CO_2 decrease and deep-water deoxygenation by iron fertilization from glaciogenic dust, Climate of the Past, 15, 981-996.

Yashayaev, I., Seidov, D., and Demirov, E.: A new collective view of oceanography of the Arctic and North Atlantic basins, Progress in Oceanography, 132, 21 pp., DOI:http://dx.doi.org/10.1016/j.pocean.2014.12.012, 2015.

Zhao, N. and Keigwin, L.D.: An atmospheric chronology for the glacial-deglacial Eastern Equatorial Pacific, Nature communications, 9:3077, DOI:10.1038/s41467-018-05574-x, 2018.

Zhao, N., Marchal, O., Keigwin, L., Amrhein, D., and Gebbie, G.: A synthesis of deep-sea radiocarbon records and their (in) consistency with modern ocean ventilation, Paleoceanography and Paleoclimatology, 33, 128-151, 2018.

TABLE CAPTIONS

~~V~~ **Table 1 a and b.** Summary of varve- and U/Th model-based age estimates (Schlolaut et al., 2018; Bronk Ramsey et al., 2012) for ~30 plateau (pl.) boundaries in the atmospheric ^{14}C record identified in Lake Suigetsu Core $SG06_{2012}$ by means of visual inspection over the interval 10.5–27 cal. ka (Sarnthein et al., 2015, suppl. and modified). At the right hand side, three columns give the average (Ø) and uncertainty range of ^{14}C ages for each ^{14}C plateau.

SUIGETSU SG06_2012 Plateau no.	Plateau Top **Varve-based** age (yr BP)	***U/Th-based*** *age (yr BP)*	Depth (cm c.d.)	Plateau Base **Varve-based** age (yr BP)	***U/Th-based*** *age (yr BP)*	Depth (cm c.d.)	Ø 14C Age of 14C Plateau (14C yr)	±Uncertainty (14C yr)	14C age BP min/max. (1.6 σ range)
'Preboreal'	10525	***10560***	1325	11100	***11108***	1383	**9525**	–170/+110	9356/ 9635
'Top YD'	11290	***11281***	1402	11760	***11755***	1453	**10060**	–100/+35	9963/ 10095
'YD'	11950	***11895***	1467	12490	***12475***	1525	**10380**	–170/ 124	10211/ 10504
'no name'	12885	***12780***	1555	13160	***13080***	1582	**11000**	–85/ 114	10915/ 11114
1a	13580	***13656***	1626	13980	***14042***	1657	**12006**	100	11857/ 12050
1	14095	***14160***	1666	15095	***15100***	1740	**12471**	185	12315/ 12683
2a	15310	***15420***	1754	16140	***16520***	1802	**13406**	245	13174/ 13665
2b	16075	***16520***	1802	16400	***16930***	1820	**13850**	40	13808/ 13885
3	16835	***17500***	1847	17500	***18220***	1888	**14671**	105	14582/ 14792
4	17880	***18650***	1913	18830	***19590***	1971	**15851**	190	15661/ 16044

5a	18960	***19720***	1978	19305	***20240***	2003	**16670**	90	16570/ 16750
5b	19305	***20240***	2003	20000	***20900***	2032	**17007**	190	16830/ 17247
6a	20190	***21000***	2050	20920	***21890***	2105	**17667**	262	17435/ 17960
6b	20920	***21890***	2105	21275	***22300***	2132	**18075**	140	17960/ 18240
7	21375	***22400***	2140	21790	***22870***	2171	**18843**	117	18741/ 18975
8	21835	***22940***	2175	22730	***24250***	2257	**19715**	–290 325	19425/ 20041
9	22730	***24250***	2257	23395	***25150***	2312	**20465**	–227 263	20238/ 20728
10a	23935	***25880***	2358	25080	***27000***	2400	**22328**	–380 270	21946/ 22600
10b	25080	***27000***	2400	25800	***27600***	2426	**22708**	–475 440	22233/ 23147
11	26110	***27770***	2443	27265	***28730***	2525	**24088**	–360 505	23727/ 24595

~~V~~ **Table 2.** Temporal match of various ^{14}C plateaus with deglacial periods of major atmospheric CO_2 rise and ocean warmings (AA = Antarctic; GIS = Greenland Interstadial).

pCO_2 RISE (~12 ppm) AGE based on annual layers AA ice core (Marcott et al. 2014)	Plateau no.	Plateau boundaries AGE range (cal. ka) based on **U/Th model ages** (Bronk Ramsey et al., 2012)
11.7 – 11.5	# 'Top YD'	**11.83 – 11.3**
14.8 – 14.53	# 1	**15.1 – 14.2**
16.4 – 16.15	# 2a	**16.52 – 15.5**
17.4 – ~17.1	(data gap)	**17.3 – 17.1**
FURTHER POTENTIAL CORRELATIVES:		
Progressive N. Atlantic warming during the YD at 12.39 – 12.03 ka *	# 'YD'	**12.46 – 11.98**
Onset of Antarctic ** warming at 18.3–17.6 ka (ice-based time scale)	#3	**18.22 – 17.5**
Onset of North Atlantic *** warming at 19.3–18.6 ka (U/Th-based time scale)	# 4	**19.6 – 18.65**
Top H2: GIS 2 N. Atlantic warming at 23.4 – 23.3 ka ****	#8	**24.25 – 22.95**

AGE CONTROL based on

* Naughton et al. (2019), ** Kawamura et al. (2007),

*** Balmer and Sarnthein (2018), **** Grootes and Stuiver (1997)

~~V~~ **Table 3** a-c. ^{14}C reservoir / ventilation ages of surface (top 50-100 m) and bottom waters vs. U/Th-based model age at 19/22 core sites in the ocean. (a) Spatial and temporal changes over early and late LGM (24–21 and 21–18.7 cal. ka), (b) HS-1, and the B/A. Late LGM estimates (average res. age of Plateau 4-5) are compared to model-based estimates of Muglia et al. (2018). (c) Data sources. For core locations see Fig. 7.

(a)

Sediment Core U/Th-based model age Plateau (Pl.) no.	Latitude	Longitude	Water depth (m)	LGM pla. res. age 24–21 ka (early LGM) Pl. 8 - 7 - 6	 Error (yr)	 21–18.7 ka (late LGM) Pl. 5 - 4	 Error (yr)	LGM model res. age strong AMOC (yr)	 weak (yr)
ATLANTIC O.									
PS2644	67°52.02'N	21°45.92'W	777	2100	±390	1920–2200	±325 –±125	1136	1100
GIK 23074	66°66.67'N	4°90'E	1157	620–790	±145–±270	550–1175	±100–±200	1054	1059
MD08-3180	38°N	31°13.45'W	3064	–		320–605	±125–±405	827	887
SHAK06-5K	37°34'N	10°09'W	2646	700–930		330–650		872	855
(= MD99-2334)	(37°48'N	10°10'W	3146						
ODP 1002	10°42.37'N	65°10.18'W	893	700–210	±230–±310	25 – -205	±205–±215	751	738
GeoB 3910-1	4°15'S	36°21'W	2361	–		–		779	796
GeoB 1711-4	23°17'S	12°23'W	1976	1080	±290	730–840	±240–±190	711	721
KNR 159-5-36GC	27°31'S	46°48'W	1268	540	±140	870	±120	757	777
MD07-3076	44°4'S	4°12'W	3770	–		2300	±200	928	989
INDIAN O./TIMOR SEA									
MD01-2378	13°08.25'S	121°78.8'E	1783	–		2000–1700	±300–±320	885	890
PACIFIC O.									
MD02-2489	54°39.07'N	148°92.13'W	3640	–		1560–1110	±310–±335	972	965
MD01-2416	51°26.8'N	167°72.5'E	2317	–		1710	±440	1227	1202
ODP 893A	34°17.25'N	120°02.33'W	588	–		1065	±280	839	846
MD02-2503	34°16.6'N	120°01.6'W	580	–		–		839	846
GIK 17940	20°07.0'N	117°23.0'E	1727	1820–1260	±320–±230	hiatus		836	838
(= SO50-37)	18°55'N	115°55'E	2655	1820–1260				836	840
PS75/104-1	44°46'S	174°31'E,	835	1650–1280		1500		881	895
(= SO213-84)	45°7.5'S	174°34,9'E	972	1650–1280		1500		881	895
MD07-3088	46°S	75°W	1536	380		200-350		917	–
SO213-76-2	46°13'S	178°1.7´W	4339	–		1600–1560		915	842
PS97/137-1	52°39.5'S	75°33.9'E	1027	2290–2110		2400–1800		1505	1419

(b)

Sediment Core	HS-1 pla. res. age				B/A pla. res. age		LGM be. vent age		LGM b.w. model age	
U/Th-based model	18 –16.5 ka		16.5–15.5 ka		14.7 –13.6 ka		(yr)		strong AMOC	weak
Plateau (Pl.) no.	Pl. 3 - 2b (yr)	Error (yr)	Pl. 2a (yr)	Error (yr)	Pl. 1 - 1a	Error (yr)	early	late	(yr)	(yr)
ATLANTIC O.										
PS2644	1775–1660	±105–±160	1900	±355	–		345	2400	948	918
GIK 23074	1730–2000	±125–±160	670	±310	140–310	±250–±100	375	375	960	931
MD08-3180	1420–1610	±310–±160	1460	±390	630–360	±310	600	600	1031	1004
SHAK06-5K	350–420		550		800–1200		—		—	—
(= MD99-2334)							2200–2700	1900	—	—
ODP 1002	–100 – 20	±140	90	±345	355	±200	—		1247	1175
GeoB 3910-1	630–560	±160–±180	175	±475	210–230	±220–±110	2150	2150	—	—
GeoB 1711-4	660–690	±195–±45	420	±320	880	±255	1500	1500	1387	1714
KNR 159-5-36GGC	460–340	±380–±300	170	±700	180–230	±370–±310	1470	1470	1354	1563
MD07-3076	1650	±180	–		920	±230	3640	3640	1653	2060
INDIAN O./TIMOR SEA										
MD01-2378	740	±125	–		200–185	±345–±135	2720	—	1679	1881
PACIFIC O.										
MD02-2489	800–550	±155–±120	550	±305	440	±285		2625	2332	2595
MD01-2416	1480–1140	±135–±195	–		720–570	±285–±140		3700/510	2400	2683
ODP 893A	1065–1490	±280–±125	1400	±370	520	±185		1430	1677	1705
MD02-2503	965–1365	±160–±165	1215	±325	395–535	±240–±130	—	—	—	—
GIK 17940	1210–1370	±200–±470	1045	±320	870–970	325–±100	3300–1800		1807	1897
(= SO50-37)							3225	3225	2373	2667
PS75/104-1	1050		1100		800–250		—	—	—	—
(= SO213-84)							1500	2400	1101	1146
MD07-3088	800–1090		1010		730–940		1600	1600	1808	1701
SO213-76-2	200		–		–		4685	4685	1712	2001
PS97/137-1	1500–670		435		–		3300	2100	1631	1871

(c)

Sediment Core	DATA Source	
ATLANTIC O.		
PS2644	Sarnthein et al. 2015	Be.data suppl.
GIK 23074	Sarnthein et al. 2015	
MD08-3180	Balmer et al. 2018	
SHAK06-5K	Ausin et al., 2019	
(= MD99-2334)	Skinner et al. 2014	
ODP 1002	Sarnthein et al. 2015	
GeoB 3910-1	Balmer et al. 2016	
GeoB 1711-4	Balmer et al. 2016	
KNR 159-5-36GGC	Balmer et al. 2016	data suppl.
MD07-3076	Balmer et al. 2016	
INDIAN O./TIMOR SEA		
MD01-2378	Sarnthein et al. 2015	
PACIFIC O.		
MD02-2489	Sarnthein et al. 2015	
MD01-2416	Sarnthein et al. 2015	modified
ODP 893A	Sarnthein et al. 2015	data suppl.
MD02-2503	Sarnthein et al. 2015	
GIK 17940	Sarnthein et al. 2015	
(= SO50-37)	Sarnthein et al. 2015	
PS75/104-1	Küssner et al., 2018	
(= SO213-84)	Ronge et al., 2016	
MD07-3088	Küssner et al., 2019	
SO213-76-2	Küssner et al., 2019	
PS97/137-1	Küssner et al., 2019	

FIGURE CAPTIONS

– Fig. 1. Atmospheric ^{14}C ages of Lake Suigetsu plant macrofossils 10–20 cal. ka (bottom panel) and 19–29 cal. ka (top panel) vs. U/Th-based model age (blue dots; Bronk Ramsey et al., 2012). The 1:1 line reflects gradient of one ^{14}C yr / cal. yr. Double and triple ^{14}C measurements are averaged. (In part large) error bars of single ^{14}C ages are given in Suppl. Fig. S1. Suite of labeled horizontal boxes that envelop scatter bands of largely constant ^{14}C ages shows ^{14}C plateaus longer than 250 yr (plateau boundary ages listed in Table 1). Red and brown dots (powder samples from trench and wall) and + signs (off-axis samples) depict raw ^{14}C ages of Hulu stalagmites H82 and MSD (Cheng et al., 2018; Southon et al., 2012; plot offset by +3000 ^{14}C yr). Suite of short ^{14}C plateaus (black boxes) tentatively assigned to Hulu-based record occupies age ranges slightly different from those deduced for Suigetsu-based plateaus. The difference possibly results from short-term changes in the Old / Dead Carbon Fraction (ocf / dcf) that in turn may reflect major short-term changes in LGM and deglacial monsoon climate (Wang et al., 2001; Kong et al., 2005).

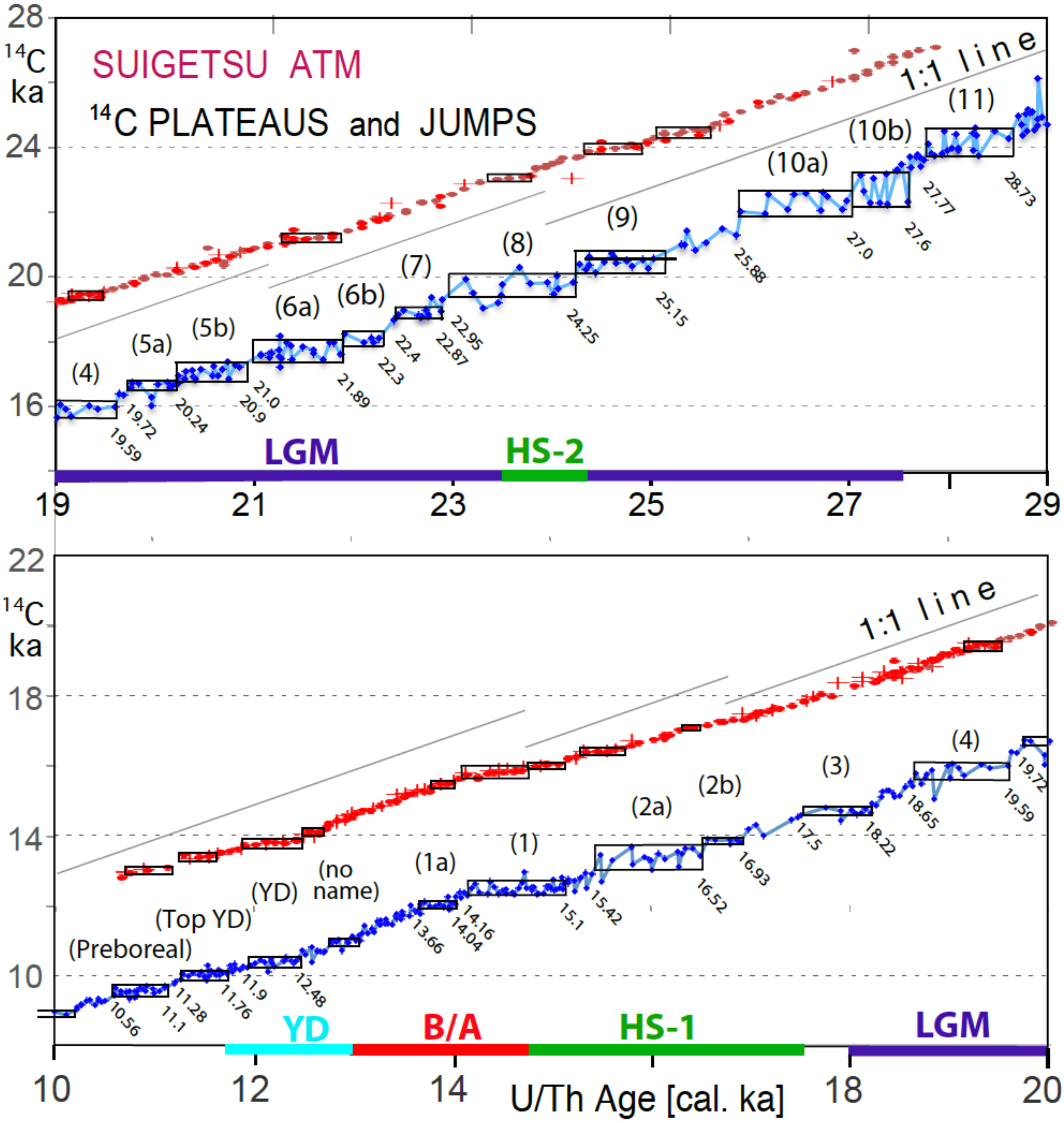
SUIGETSU ATM
^{14}C PLATEAUS and JUMPS
^{14}C ka
1:1 line
(4)
(5a)
(5b)
(6a)
(6b)
(7)
(8)
(9)
(10a)
(10b)
(11)
19.59
19.72
20.24
20.9
21.0
21.89
22.3
22.4
22.87
22.95
24.25
25.15
25.88
27.0
27.6
27.77
28.73
LGM
HS-2
28
24
20
16
19
21
23
25
27
29
22
18
14
10
(Preboreal)
(Top YD)
(YD)
(no name)
(1a)
(1)
(2a)
(2b)
(3)
10.56
11.1
11.28
11.76
11.9
12.48
13.66
14.04
14.16
15.1
15.42
16.52
16.93
17.5
18.22
18.65
19.59
19.72
YD
B/A
HS-1
LGM
12
14
U/Th Age [cal. ka]
18
20

Fig. 2. High-resolution record of atmospheric ^{14}C jumps and plateaus (= suite of labeled horizontal boxes that envelop scatter bands of largely constant ^{14}C ages extending over >300 cal. yr) in a sediment section of Lake Suigetsu vs. tree ring-based ^{14}C jumps and plateaus 10–14.5 cal. ka (Reimer et al., 2013). Blue line averages paired double and triple ^{14}C ages of Suigetsu plant macrofossils. Age control points (cal. ka) follow varve counts (Schlolaut et al., 2018) and U/Th model-based ages of Bronk Ramsey et al. (2012). YD = Younger Dryas, B/A = Bølling-Allerød.

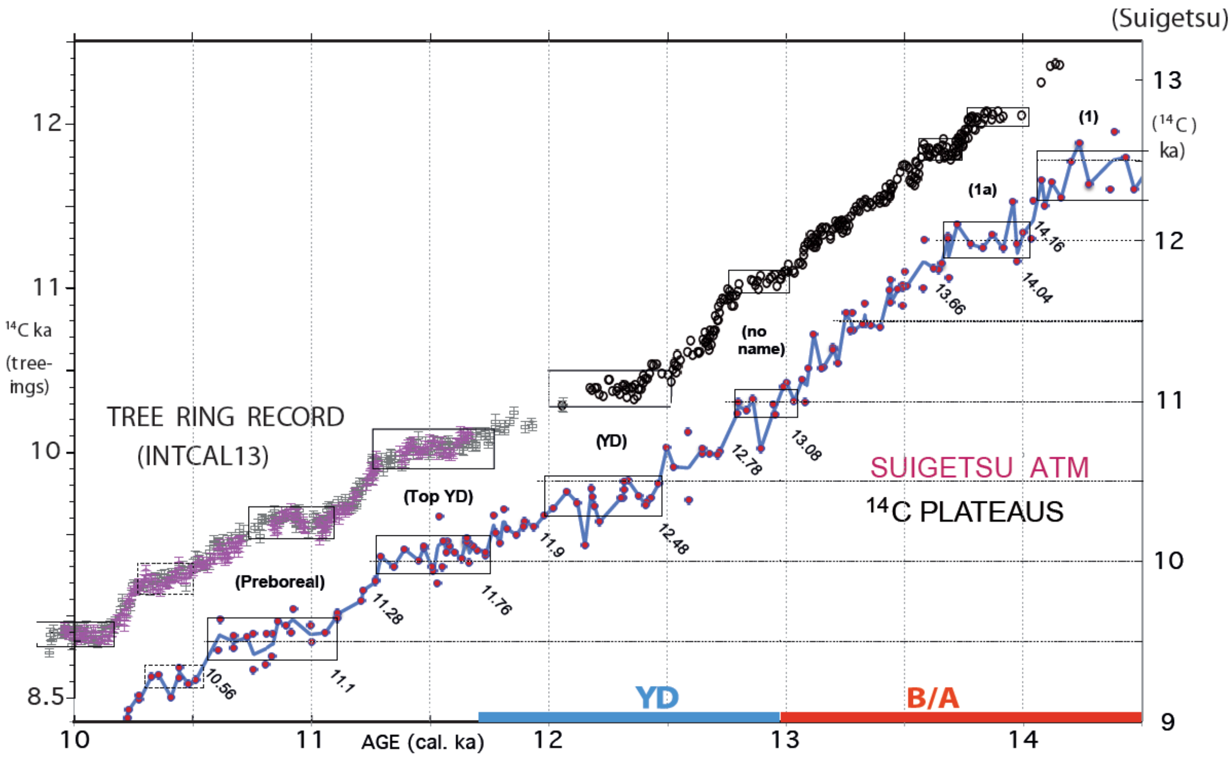

~~V~~ Fig. 3. Difference between Hulu Cave U/Th-based model ages (Southon et al., 2012; Bronk Ramsey et al., 2012; Cheng et al., 2018) and varve count-based cal. ages for atmospheric ^{14}C plateau boundaries in Lake Suigetsu sediment record (Schlolaut et al., 2018) (Sarnthein et al., 2015, suppl. and revised), displayed on the U/Th-based time scale 13–27 cal. ka.

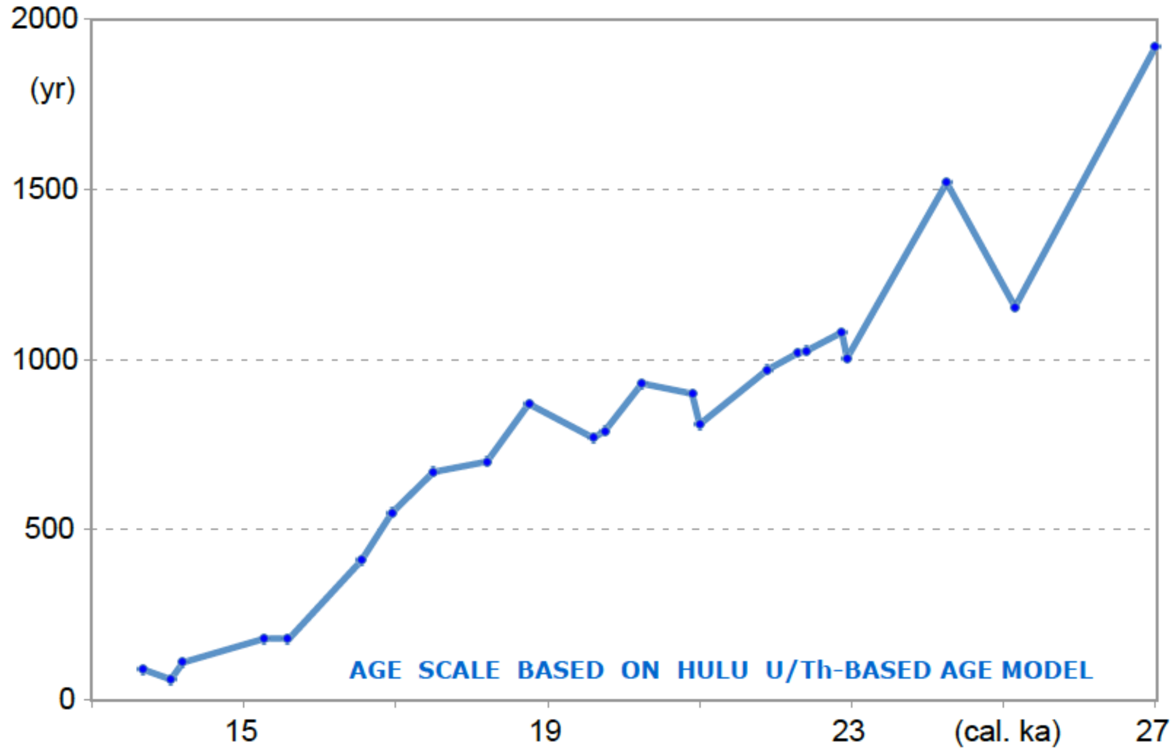

~~V~~ Fig. 4 a and b. Atmospheric ^{14}C ages and plateaus (horizontal boxes) deduced from ^{10}Be production rates vs. GICC05 age scale (Adolphi et al., 2018) compared to the Suigetsu record of atmospheric ^{14}C plateaus vs. Hulu U/Th-based model ages (Southon et al., 2012; Cheng et al., 2018) for the intervals a) 10-20 and b) 19-29 cal ka BP.

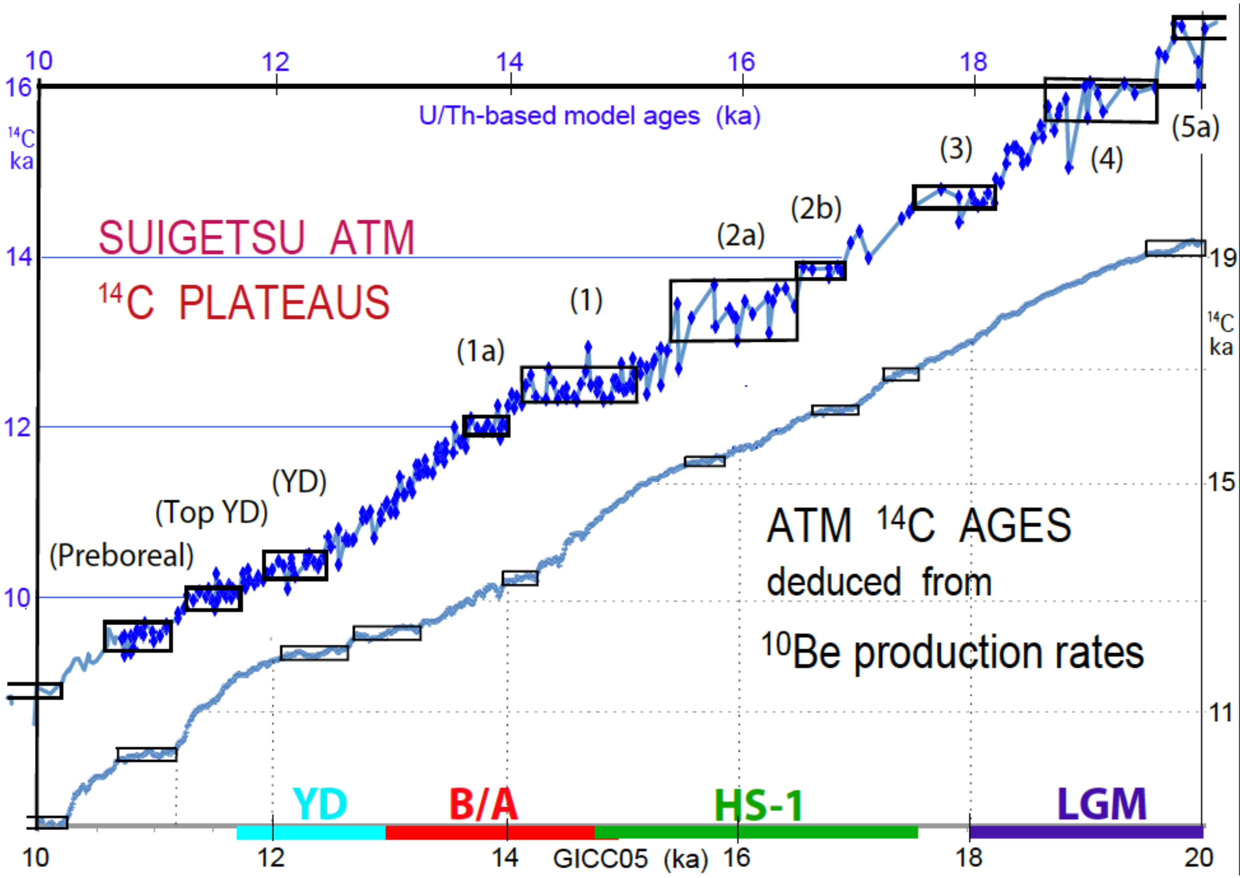

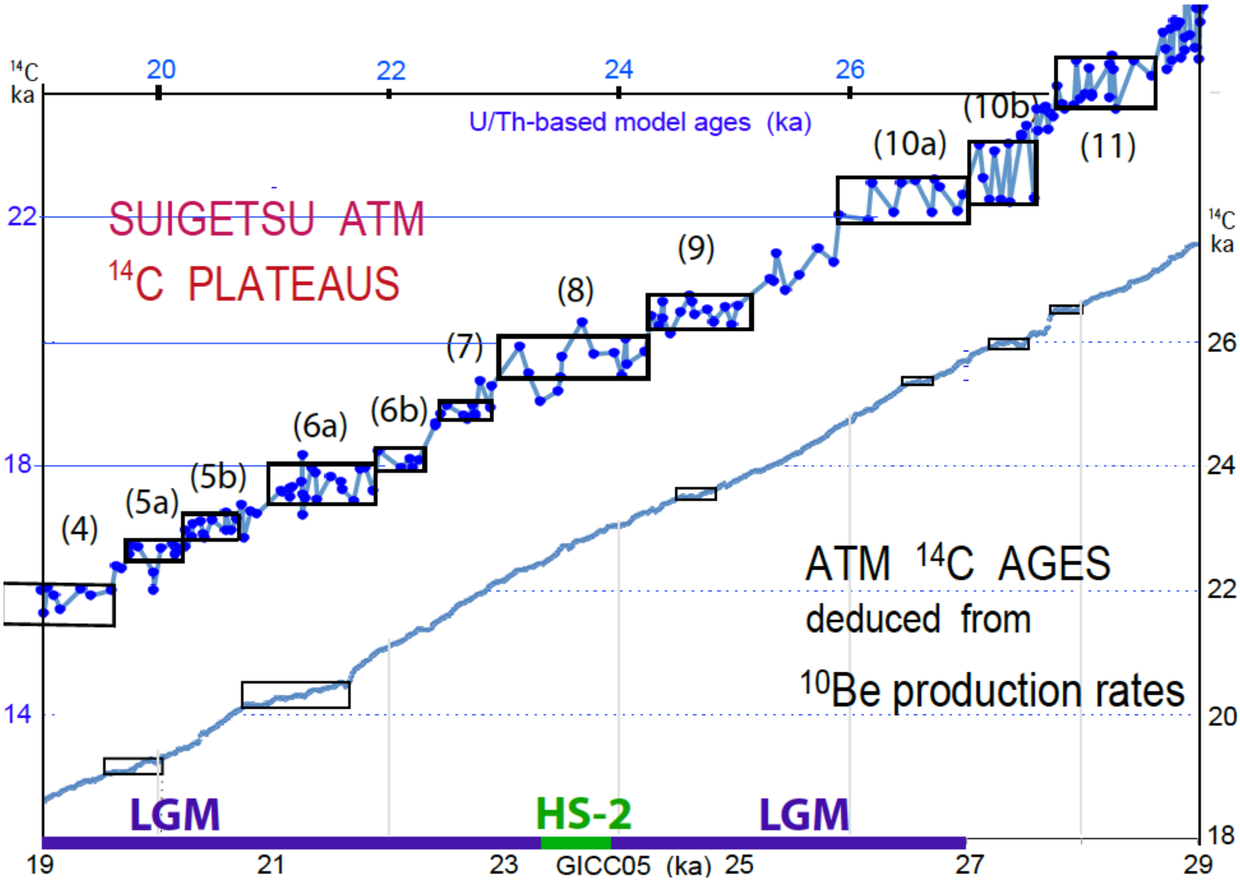
SUIGETSU ATM
14C PLATEAUS
U/Th-based model ages (ka)
ATM 14C AGES
deduced from
10Be production rates
(4)
(5a)
(5b)
(6a)
(6b)
(7)
(8)
(9)
(10a)
(10b)
(11)
LGM
HS-2
LGM
14C ka
GICC05 (ka)

√ Fig. 5. Sediment facies and microfacies zones in Lake Suigetsu Core SG06, ~13–32 m depth (simplified and suppl. from Schlolaut et al., 2018). Microscopy-based frequency of siderite layers with quality level 1–3 (= running average of layer counts per 20 cm thick sediment section) serves as measure of seasonal lamination quality and shows gradual transitions between varved and poorly varved sediment sections. Rounded varve ages are microscopy based and constrain age of major facies and microfacies boundaries. ANI I to ANI III mark core sections with ultrafine lamination due to sedimentation rate minima, AT marks tephra layer named AT, 'Event layers' label major thin mud slides probably earth quake-induced.s

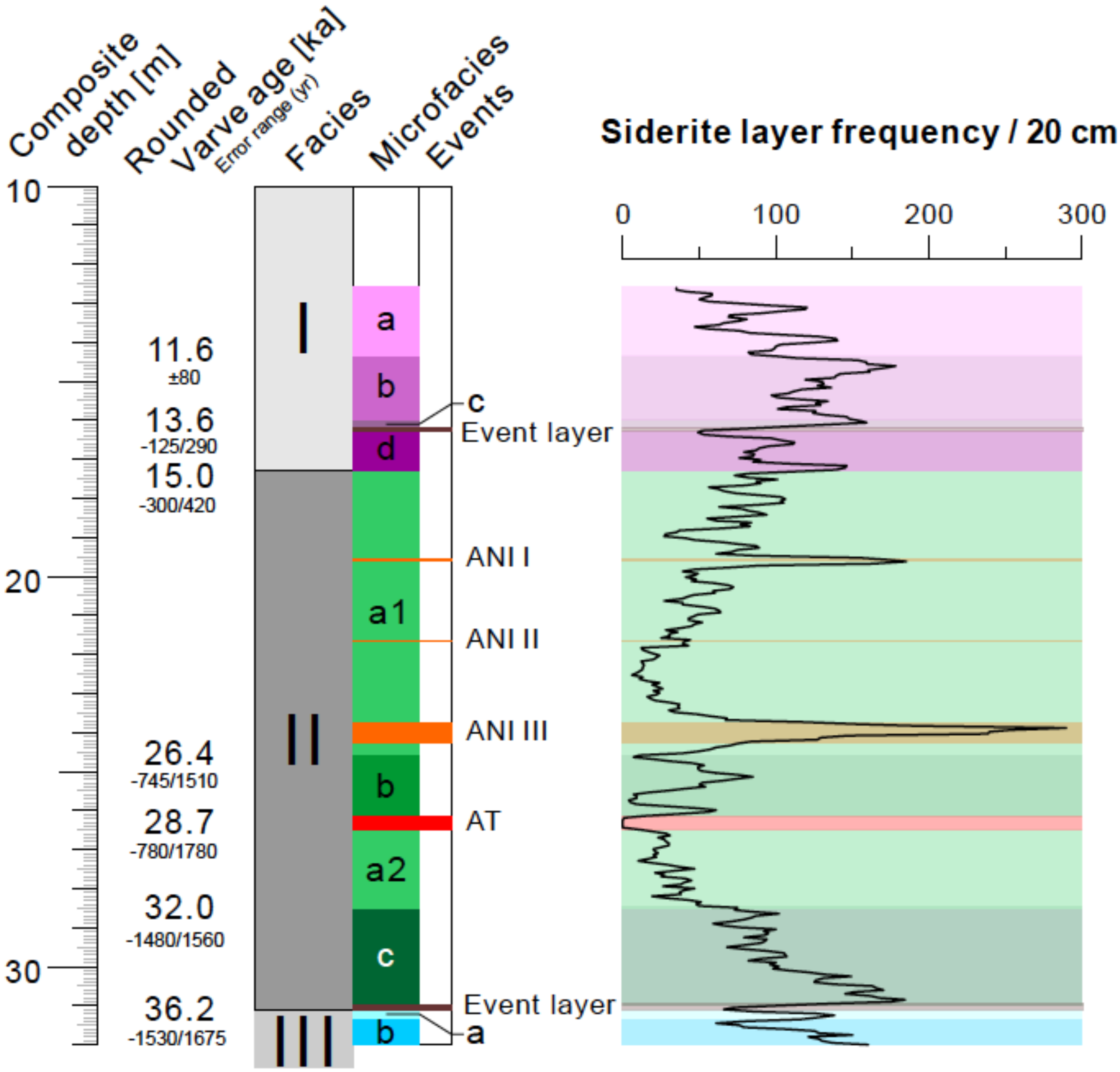

Fig. 6 (a). Four sudden steps (pink bars) in the deglacial atmospheric CO_2 rise at West Antarctic Ice Sheet Divide ice core (WDC) reflect events of fast ocean degassing, that may have contributed to the origin of deglacial ^{14}C plateaus. Age control based on ice cores (Marcott et al., 2014). (b) The steps are compared to suite of atmospheric ^{14}C plateaus dated by Hulu U/Th-based model ages (Bronk Ramsey et al., 2012). Hol = Holocene; YD = Younger Dryas; B/A = Bølling-Allerød; HS = Heinrich stadials 1 and 2; LGM = Last Glacial Maximum, GIS-2 = Greenland interstadial 2.

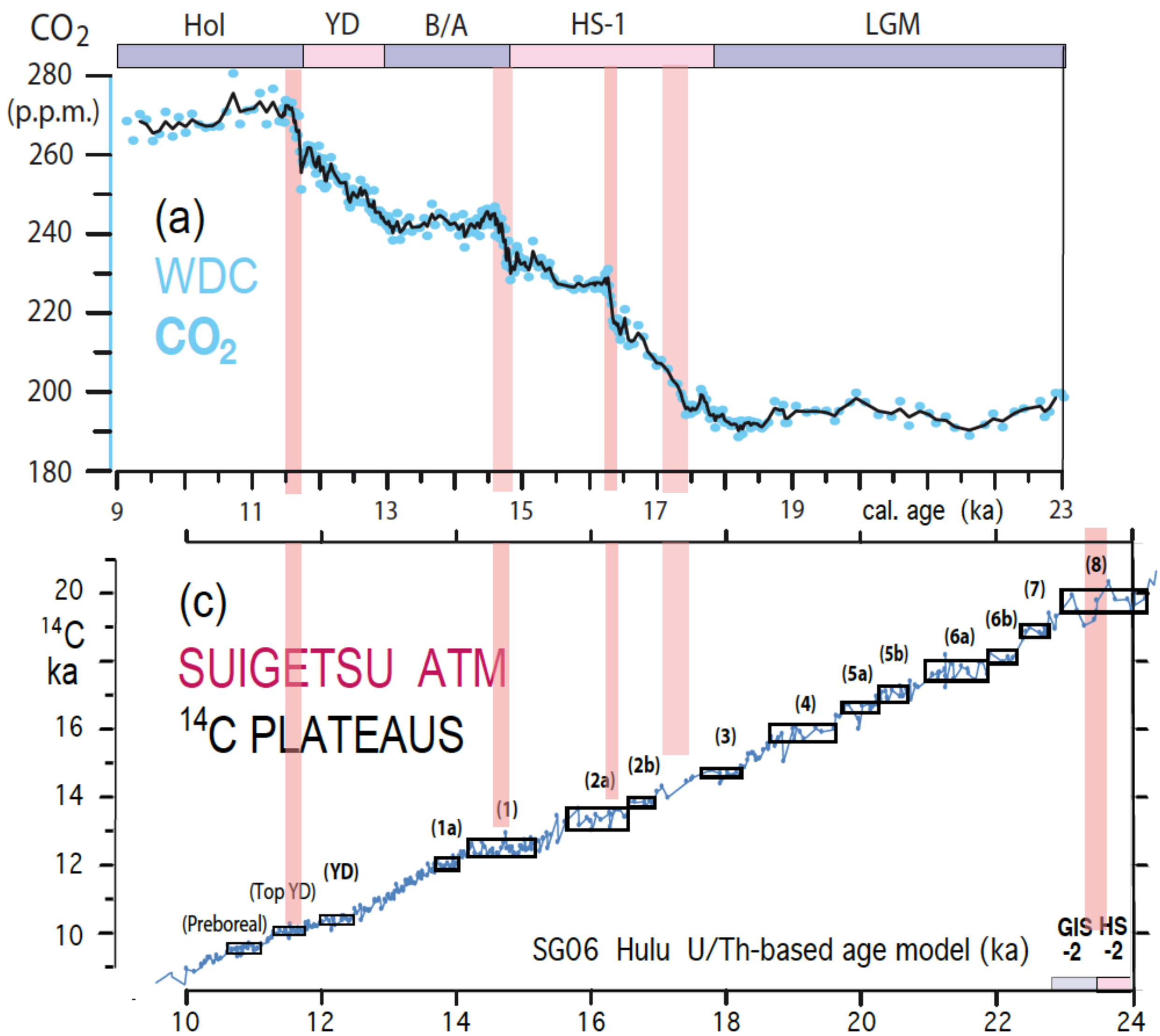

Fig. 7. Location (a) and water depth (km) (b) of sediment cores with age control based on ^{14}C plateau tuning. ^{14}C reservoir ages of cores labeled with 'w' are derived from samples with paired wood chunks and planktic foraminifers.

(a)

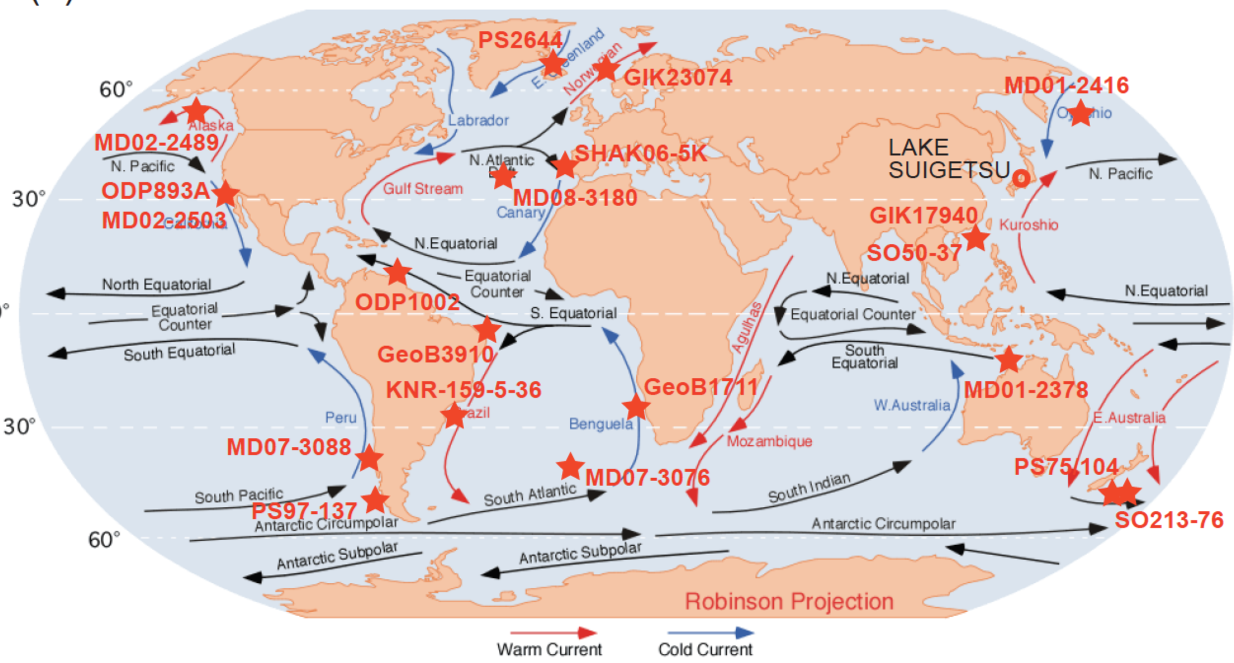

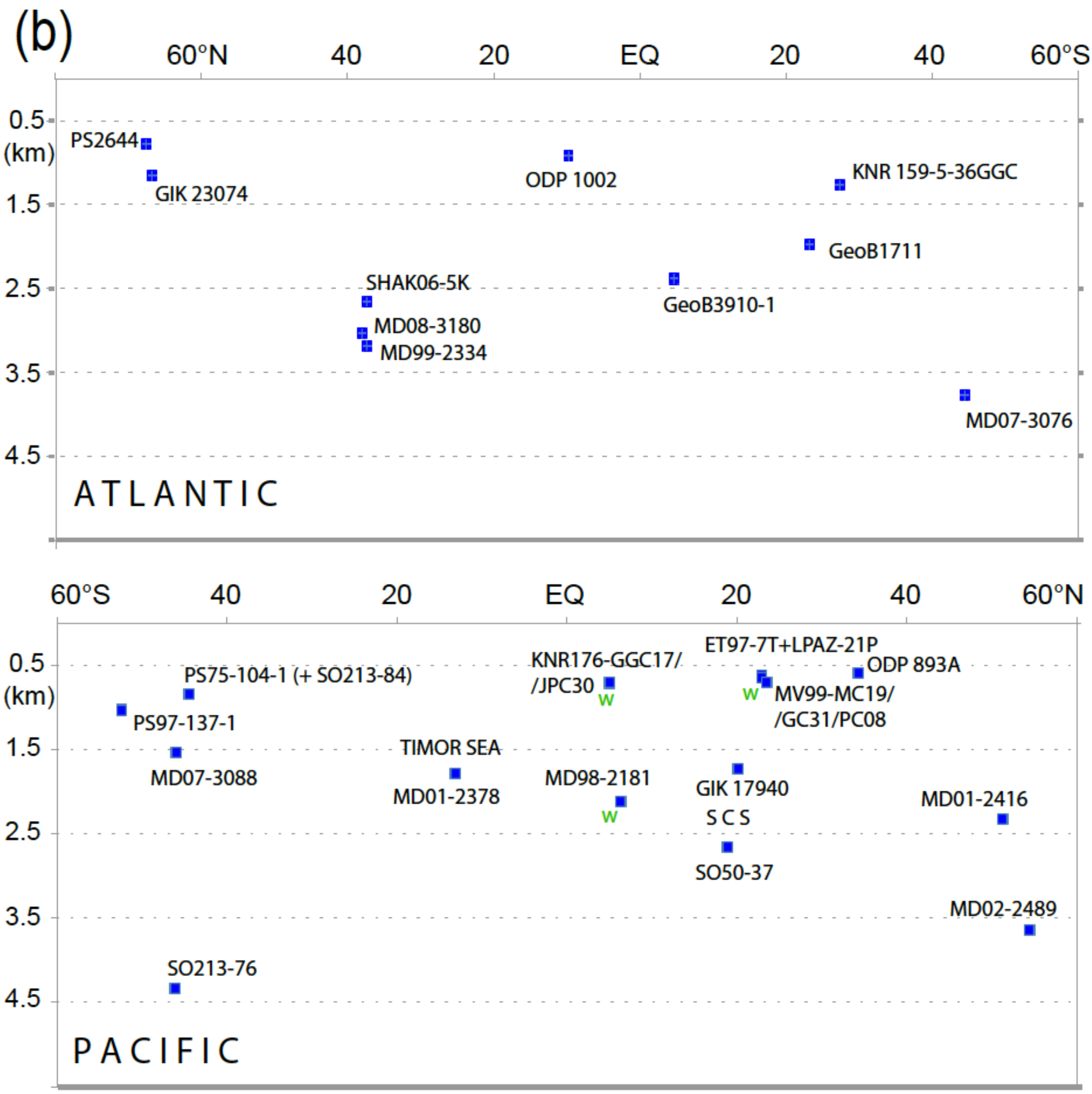

~~V~~ Fig. 8. Global distribution of ^{14}C reservoir ages of Late LGM surface waters estimated (a) by means of ^{14}C plateau tuning of planktic 14C records. (b) Model-based estimates (GCM of Muglia et al., 2018, assuming an AMOC strength of 13 Sv) for sites with planktic foraminifera-based age values. X-Y graph (c) and map (d) show (rounded) differences between observed and modeled values and their intra-LGM trends. Minor differences are displayed in magenta, larger differences of >400 yr in red. Planktic habitat depths and model estimates are largely confined to 0–100 m water depth.

Arrows of surface currents delineate different sea regions important to assess potential limits of spatial extrapolation of reservoir ages. Distribution of core numbers and references for ^{14}C records are given in Table 3a-c and Fig. 7a.

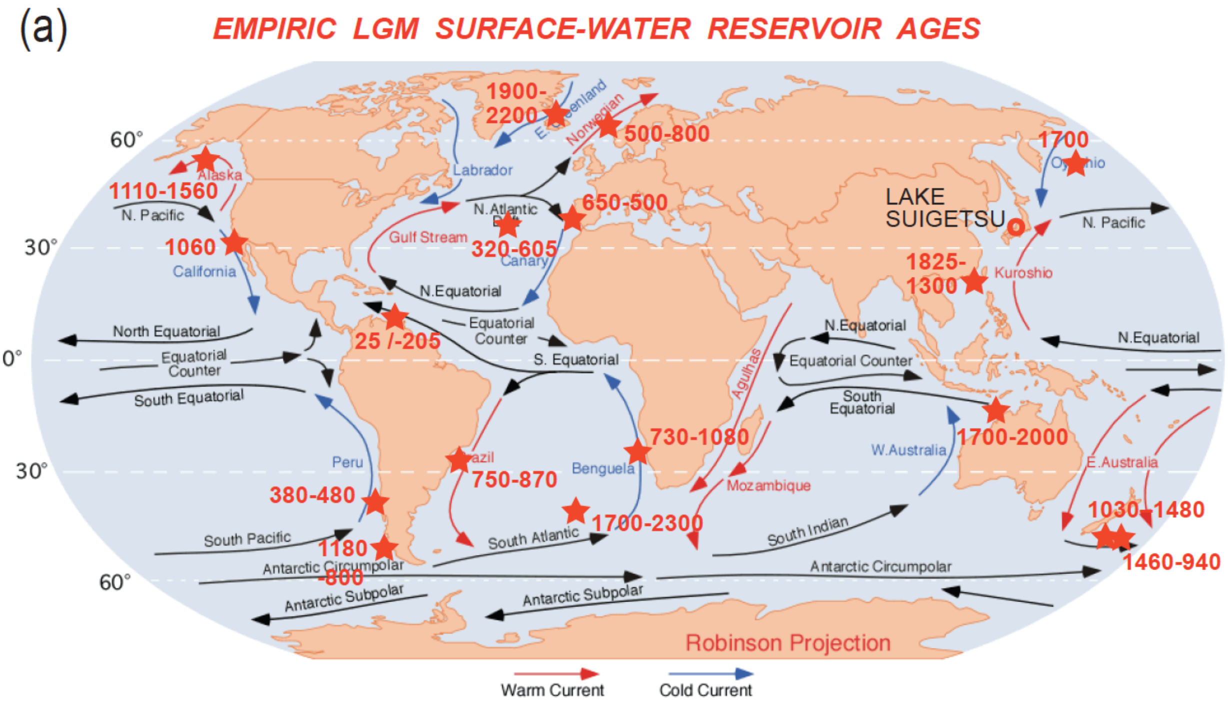

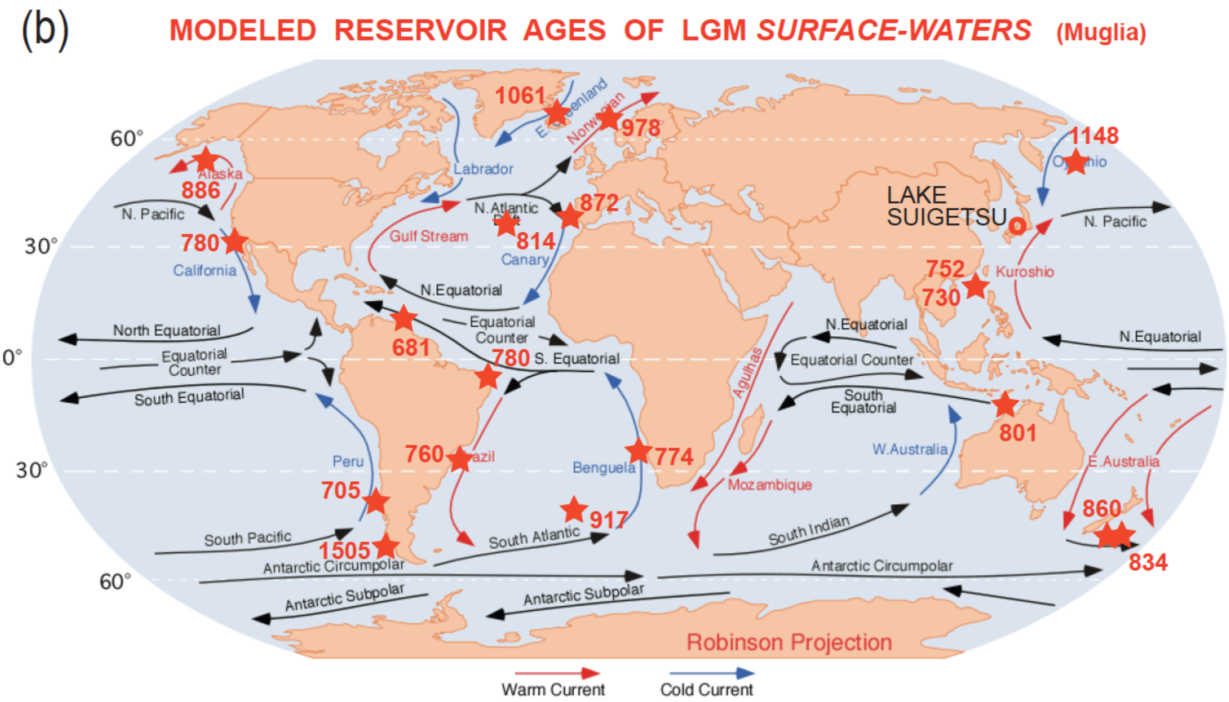

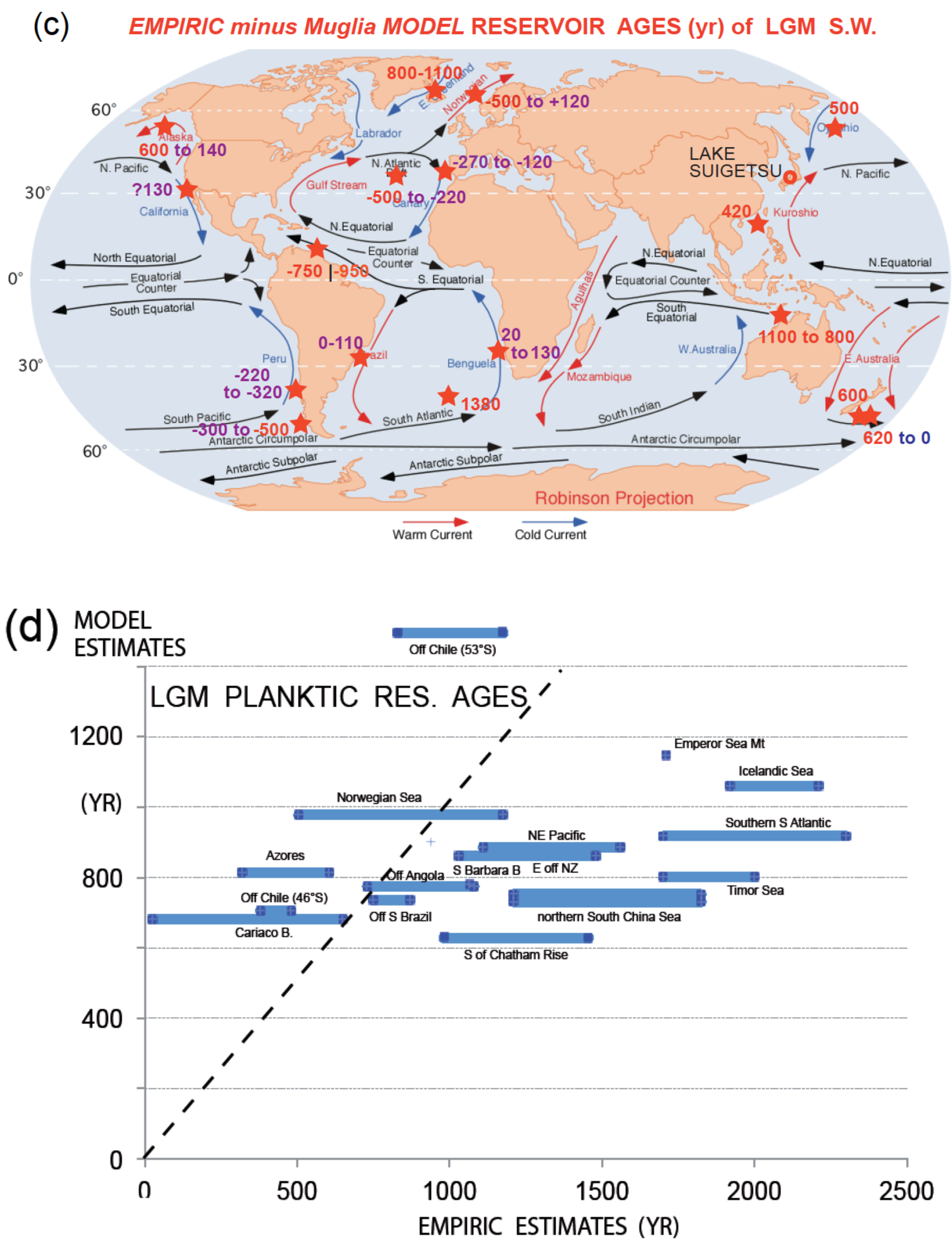

~~V~~ Fig. 9. SW–NE transect of ^{14}C reservoir age and changes in ventilation age across sites GIK17940 and SO50-37 in the South China Sea during late LGM (^{14}C Plateaus 5 and 4; upper panel) and HS-1 (lower panel). Insert map shows location of transect and core locations. Core locations are given in Fig. 7. An extreme epibenthic $\delta^{13}C$ minimum in far southwest (Core GIK17964; Sarnthein et al., 1999) reflects an LGM incursion of Lower/Upper Pacific Deep Waters (L./ U. PAC DW) with extremely high ^{14}C ventilation age and DIC enrichment in contrast to a low ventilation age of North Pacific Deep Water (N. PAC DW). Arrows show direction of potential deep and intermediate-water currents.

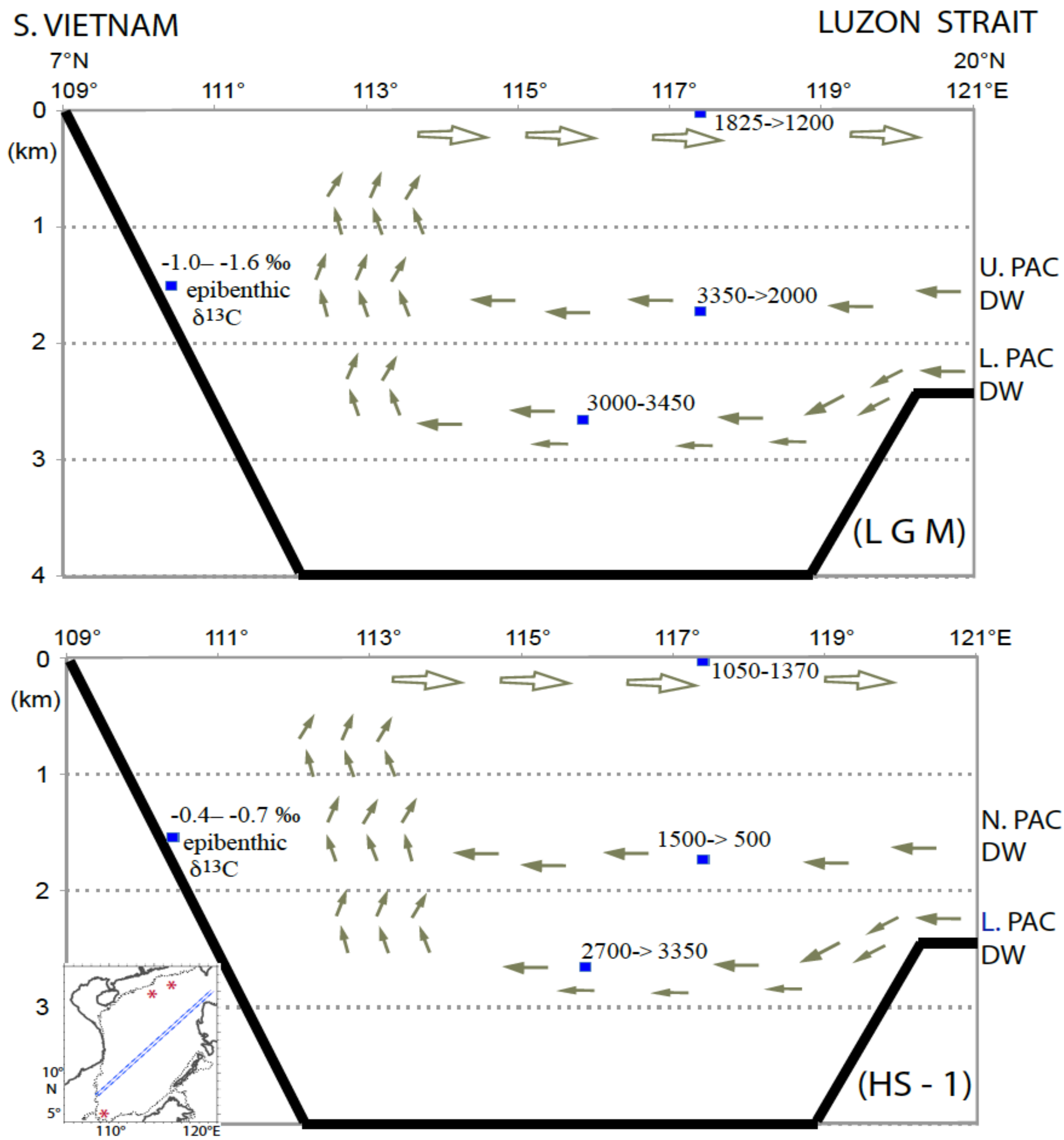

~~V~~ Fig. 10. 2D transects of the geometries of global ocean MOC. Arrows (blue = high, yellow = poor ventilation) suggest average deep and intermediate-water currents that follow the gradient from low to high benthic ventilation ages based on paired planktic ^{14}C reservoir ages derived by means of ^{14}C plateau tuning technique (Sarnthein et al., 2013, Balmer et al., 2018, Küssner et al., in prep.). Reservoir ages at some Pacific sites are based on paired ^{14}C ages of planktic foraminifera and wood chunks (marked by green 'w'; Sarnthein et al., 2015; Zhao and Keigwin, 2018, Rafter et al., 2018). Red arrows suggest poleward warm surface water currents. Zigzag lines mark location of major frontal systems separating counter rotating ocean currents (e.g., W of Portugal and N of MD07-307; after Skinner et al., 2014). (a) Late LGM circulation geometry, largely similar as today. Note the major east-west gradient of ventilation ages in the central North Atlantic, between Portugal (PORT) and Mid-Atlantic Ridge W of Azores (MAR)). (b) HS-1 benthic ventilation ages reveal a short-lasting MOC reversal leading to Atlantic-style overturning in the subpolar North Pacific and coeval Pacific-style stratific-ation in the northern North Atlantic, with seesaw-style reversals of global MOC at the onset and end of early HS-1 (first proposed by Broecker et al., 1985, however, for LGM times). Increased ventilation ages reflect enhanced uptake of dissolved carbon in the LGM deep ocean (Sarnthein et al., 2013), major drops suggest major degassing of CO_2 from both the deep Southern Ocean and North Pacific during early HS-1. – SCS = South China Sea. AABW = Antarctic Bottom Water; AAIW = Antarctic Intermediate Water. NADW = North Atlantic Deep Water. Small arrows within age numbers reflect temporal trends. Many arrows are speculative using circumstantial evidence of benthic $\delta^{13}C$ records and local Coriolis forcing at high-latitude sites per analogy to modern scenarios. Location of sediment cores are given in Fig. 7, short-term variations in planktic and benthic ^{14}C reservoir/ventilation age in Suppl. Fig. S2 and Table 3.

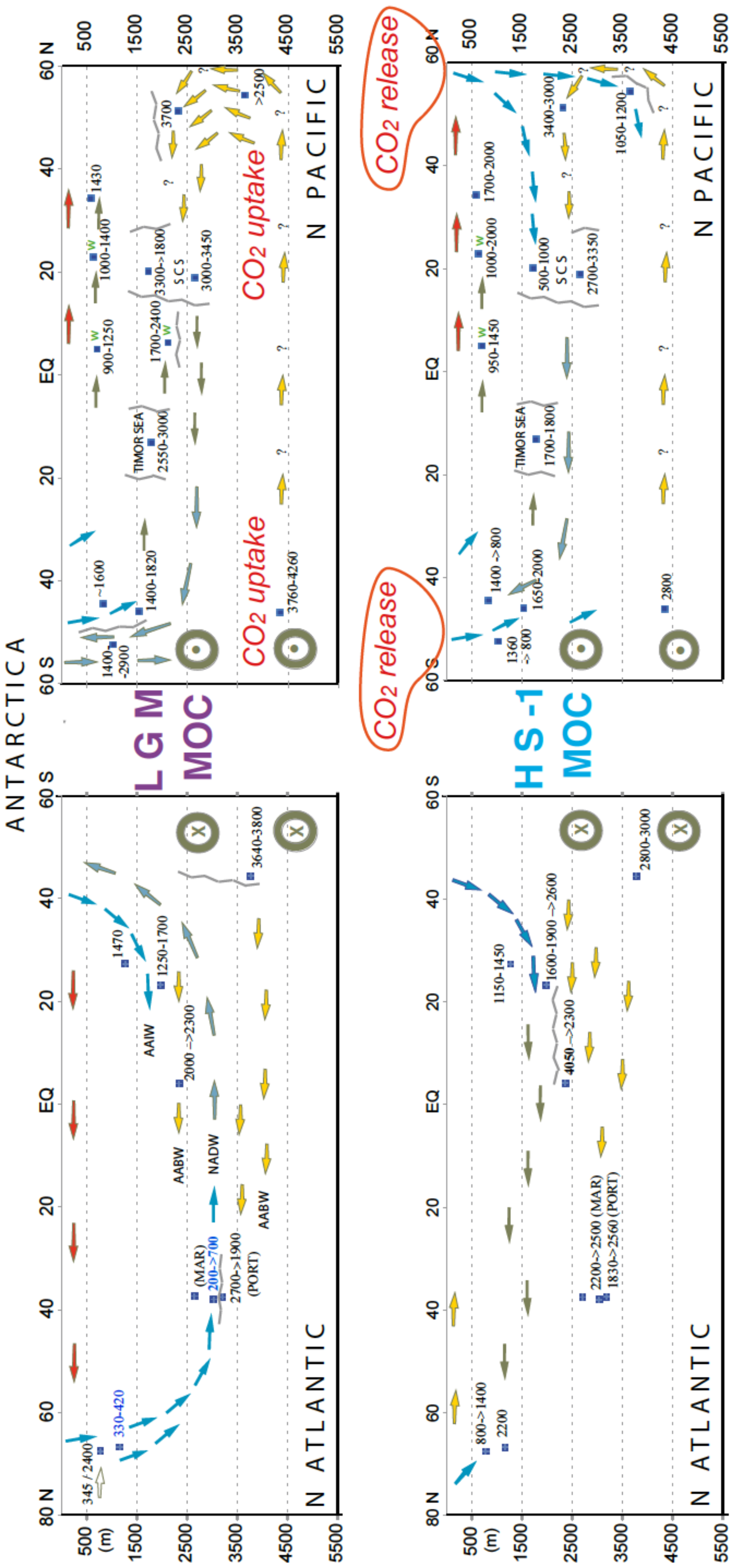
ANTARCTICA
L G M
MOC
H S -1
MOC
N PACIFIC
N ATLANTIC
CO_2 uptake
CO_2 uptake
CO_2 release
CO_2 release
AAIW
AABW
NADW
AABW
TIMOR SEA
S C S
(m)
80 N
60
40
20
EQ
20
40
60 S
60 N
500
1500
2500
3500
4500
5500

~~V~~ Fig. 11. Global distribution of ^{14}C reservoir ages obtained (a) for late LGM intermediate waters (100–1800 m w.d.) and (b) for LGM deep waters (>1800 m w.d., including Site GIK 23074 at 1157 m in the Norwegian Sea).

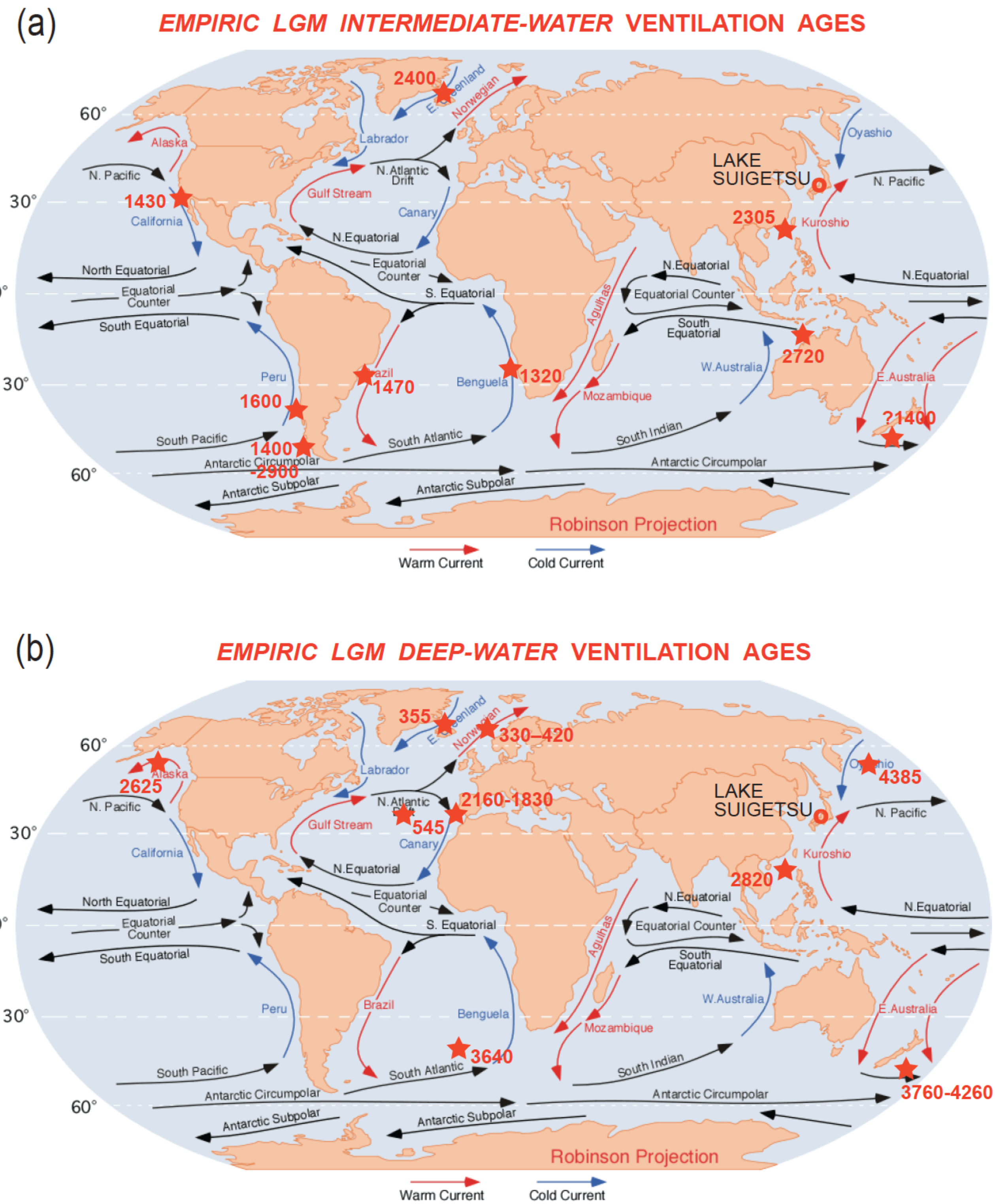

1394

Plateaus and jumps in the atmospheric radiocarbon record – Potential origin and value as global age markers for glacial-to-deglacial paleoceanography, a synthesis

Michael Sarnthein[1)], Kevin Küssner[2)], Pieter M. Grootes[3)], Blanca Ausin[4)8)], Timothy Eglinton[4)], Juan Muglia[5)], Raimund Muscheler[6)], Gordon Schlolaut[7)]

Supplementary Materials

SUPPLEMENTARY TEXT #1. Uncertainties of age control

Rough estimates of uncertainty and aspects of analytical quality were published by Sarnthein et al. (2007, 2015). We now focus on uncertainties tied to the calendar age definition for each ^{14}C plateau boundary both in the Suigetsu atmospheric and the various marine sediment records (Table 1). To recap, an age/sediment section is formally defined as containing a '^{14}C plateau', when ^{14}C ages show almost constant values with an overall gradient of <0.3 to <0.5 ^{14}C yr per cal. yr (based on visual description and/or statistical estimates by means of the 1st derivative of all downcore changes in the ^{14}C age – calendar age relationship; Sarnthein et al., 2015) and a variance of less than ±100 to ±300 ^{14}C yr, and up to 500 ^{14}C yr prior to 25 cal. ka. Here ^{14}C ages form a plateau-shaped scatter band with up to 10% outliers, that extends over more than 300 cal. yr in the Suigetsu record and/or equivalent sections of marine sediment depth (following rules defined by Sarnthein et al., 2007).

On visual inspection a plateau boundary is assigned to the break point between the low to zero or reversed slope of a ^{14}C plateau and the normally high regression slope of the ^{14}C concentration jump that separates two consecutive plateaus (Figs. 1 and S1). More precisely, a boundary marks the point, where the ^{14}C curve exceeds the scatter band of the plateau either crossing the upper or lower envelope line. Thus, the boundary is chosen about halfway between the last ^{14}C age within a plateau band and the next following age outside the scatter band (Figs. 1 and 2). On the U/Th-based model age scale (Bronk Ramsey et al., 2012) most ^{14}C dates of the Lake Suigetsu section are spaced at intervals of <10–60 yr from 10 to 15 cal. ka and 20–140 yr between 15 and 29 cal. ka (Fig. 1). Thus the uncertainty of a plateau boundary age assigned halfway between two ^{14}C ages nearby inside and outside a plateau's scatter band would, on average, amount to ±10–±70 cal. yr.

In principle, the calendar age uncertainties of marine ^{14}C plateau boundaries are treated likewise: After being tuned to those in the Suigetsu ^{14}C record, the uncertainties are deduced for the position of all plateaus of a suite within the uncertainty envelope of the U/Th model-based age calibration. Hence the estimates of total age uncertainty present the propagated error of the calibrated age of a Suigetsu plateau boundary plus that of the pertinent plateau in the marine record, where variable depth spacing of ^{14}C ages is converted into average time spans.

SUPPLEMENTARY FIGURE CAPTIONS

~~V~~ Fig. S1. Individual atmospheric ^{14}C ages and error bars of Lake Suigetsu plant macrofossils vs. U/Th-based model age of 15–21 (bottom) and 21–27 (top) cal. ka (blue dots; Bronk Ramsey et al., 2012). ^{14}C plateaus longer than 250 yr are outlined by a suite of labeled horizontal boxes that envelop scatter bands of largely constant ^{14}C ages. Red dots and black circles in Fig. 1a display ^{14}C ages of Hulu stalagmites. Similar to ^{14}C ages of Suigetsu also those of Hulu Cave reveal a suite of ^{14}C plateaus (red boxes) tentatively assigned in this figure, plateaus that are shorter than Suigetsu-based plateaus and occupy slightly different age ranges. The 1:1 line reflects gradient of one ^{14}C yr / cal. yr.

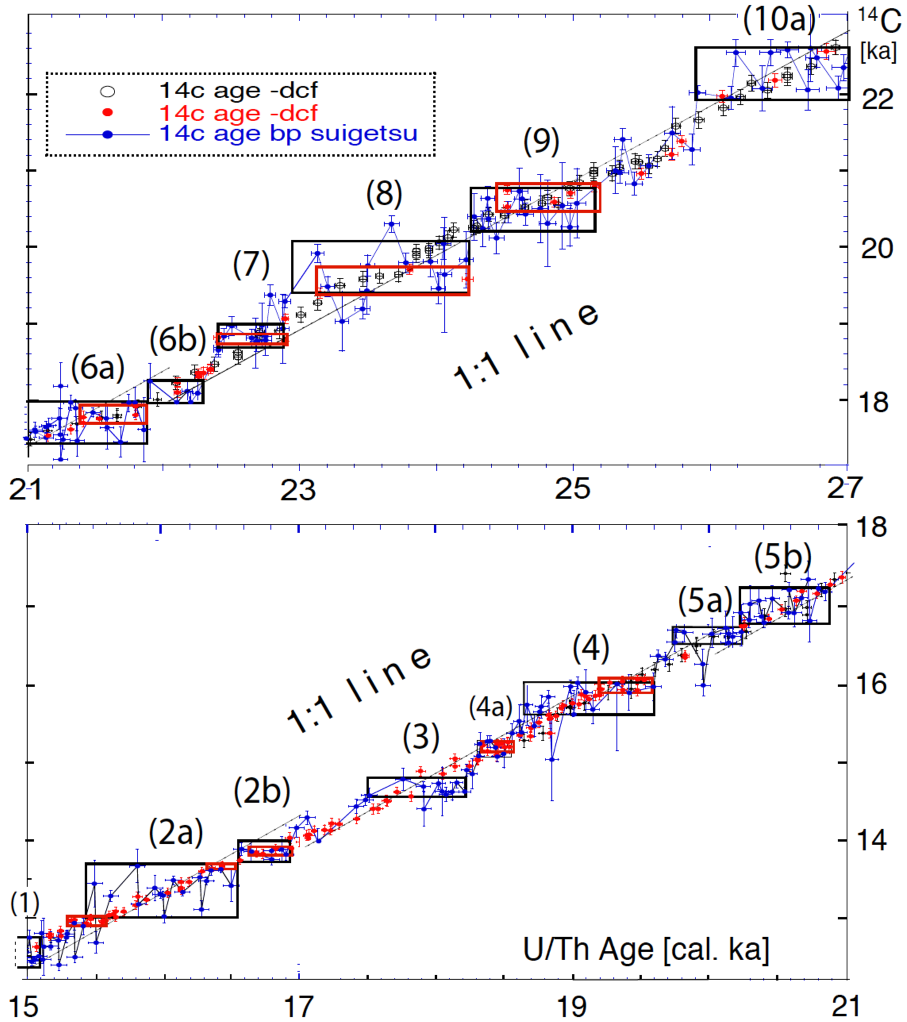

~~V~~ Fig. S2. Centennial-to-millennial-scale temporal and spatial variations in planktic (pla.) reservoir (res.) and (raw = uncorrected) apparent (app.) benthic ^{14}C ventilation (vent.) ages recorded at 18/20 key sites in the Atlantic (S2a, b, e), Pacific (S2c, d), and Indian Ocean (S2e). Site locations are given in Fig. 7. Stratigraphic units are marked on top of each diagram: Younger Dryas (YD), Bølling-Allerød (B/A) Heinrich Stadial 1 (HS-1), Last Glacial Maximum (LGM), and Heinrich Stadial 2 (HS-2).

Origin and various features characteristic of ^{14}C records: About 50% of all planktic and ('raw') benthic ^{14}C records were already published in Sarnthein et al. (2015). However, the cal. age of all records originally based on microscopy-based varve counts was now converted into U/Th-based model ages (Bronk-Ramsey et al., 2012). Planktic ^{14}C reservoir ages of Core GIK23074 are now supplemented by benthic ventilation ages stored at PANGAEA databank. Planktic ^{14}C reservoir ages of SHAK06-5K are detailed in Ausin et al. (2019, unpubl., and data stored under embargo at PANGAEA). Benthic ventilation ages plotted for SHAK06-5K are matched from neighbor core MD99-2334K (Skinner et al., 2014) the stratigraphy and ^{14}C reservoir ages of which are closely correlated by means of narrow-spaced suites of ^{14}C ages. To show an example, 'raw' benthic ventilation ages in Core MD08-3180 are recalculated into 'actual' ventilation ages (Balmer and Sarnthein, 2018) that incorporate past changes in atmospheric ^{14}C concentration between the time of deep-water formation and the local growth of benthic foraminifers. South Atlantic ^{14}C records GeoB3910, GeoB1711-4, and KNR-159-5-36 (data slightly supplemented) are from Balmer et al. (2016), now however, with cal. ages converted into U/Th based model ages. The same applies to MD07-3076, where the continuous planktic and benthic ^{14}C records are from Skinner et al. (2010), corroborated by three blue bars reflecting the extent of planktic ^{14}C plateaus tuned to atmospheric plateaus no. 1, 2b, and 4. South Pacific ^{14}C records PS75-104, SO213-76, MD07-3088, and PS97-137-1 are from Küssner et al., 2018, and data stored under embargo at PANGAEA). Planktic and benthic ^{14}C records of neighbor cores GIK17940 and SO50-37, PS75-104 and SO213-84, and ODP893A and MD02-2503 each are plotted on joint graphs, paired records that are obtained from small-scale sea regions with a common level of planktic ^{14}C reservoir age. Benthic ^{14}C ages of SO50-37 and SO213-84 are from Ronge et al. (2016), those of MD07-3088 from Siani et al. (2013).

Fig. S2a. NORTH ATLANTIC AND NORDIC SEA SITES

WEST and CENTER — *— EAST*

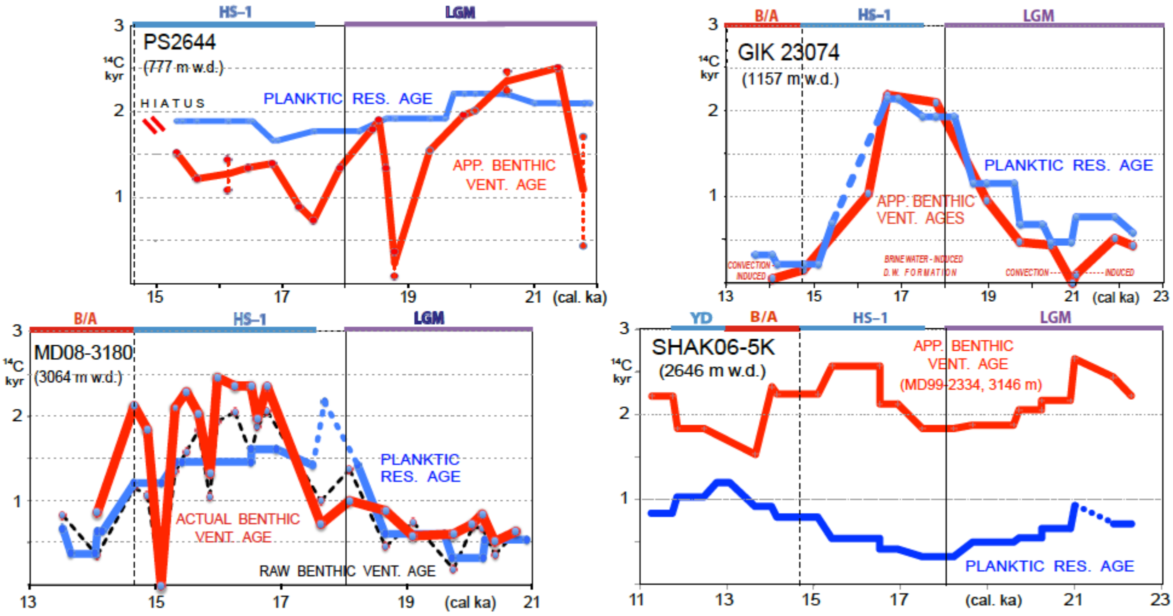

Fig. S2b. SOUTH ATLANTIC SITES

WEST — *— CENTER and EAST*

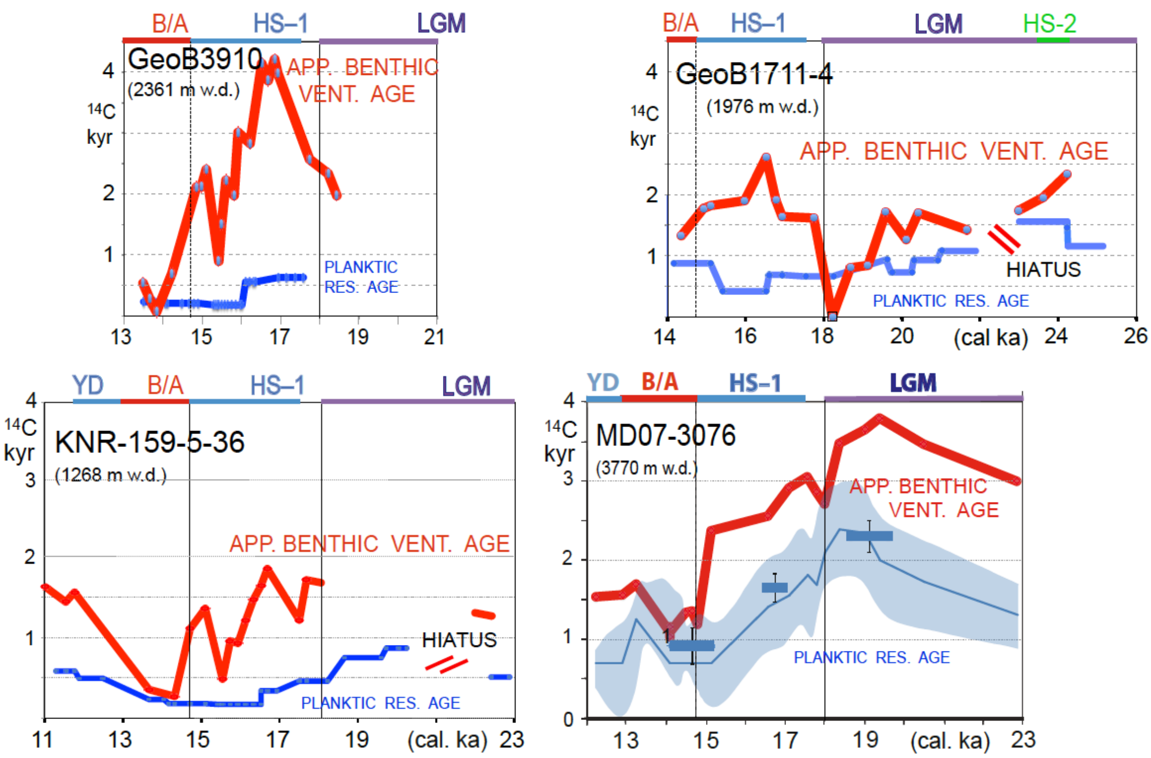

Fig. S2c. SOUTH PACIFIC SITES

WEST — *— EAST*

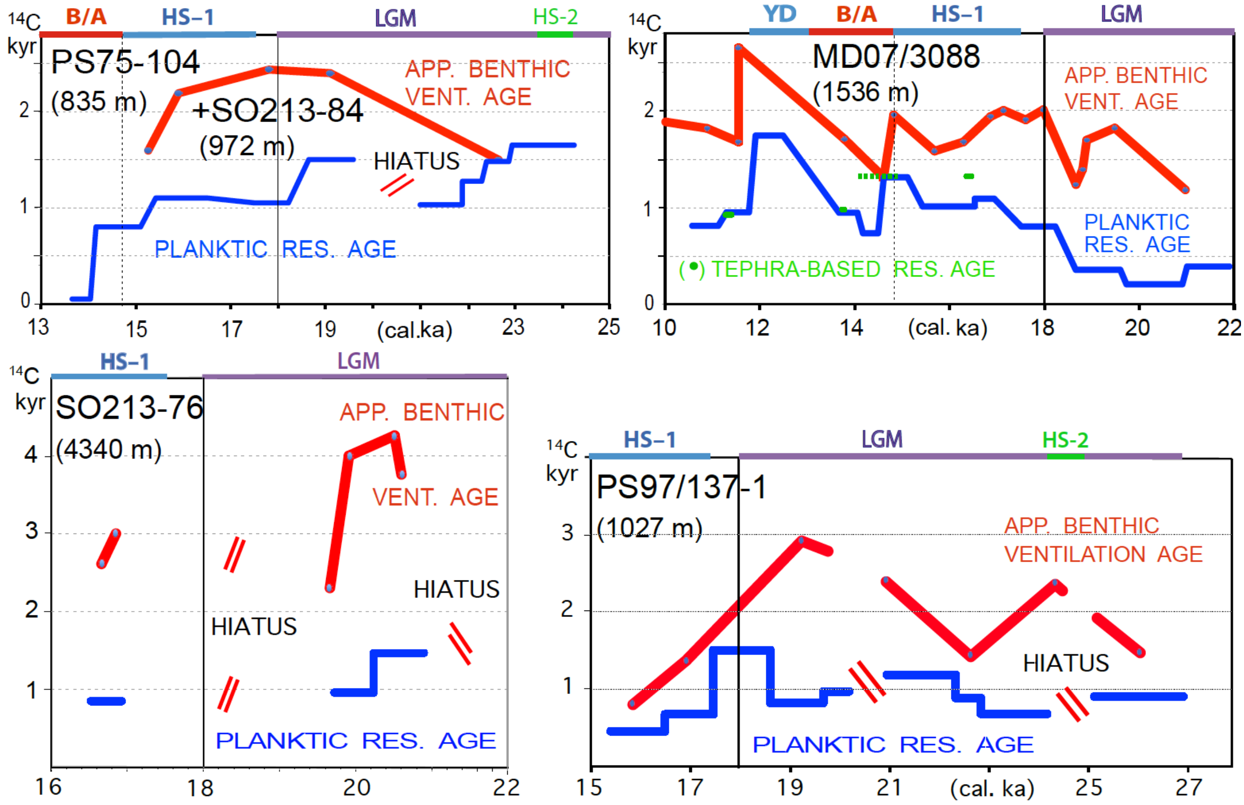

Fig. S2d. NORTH PACIFIC SITES

WEST and SOUTH CHINA SEA — *— EAST*

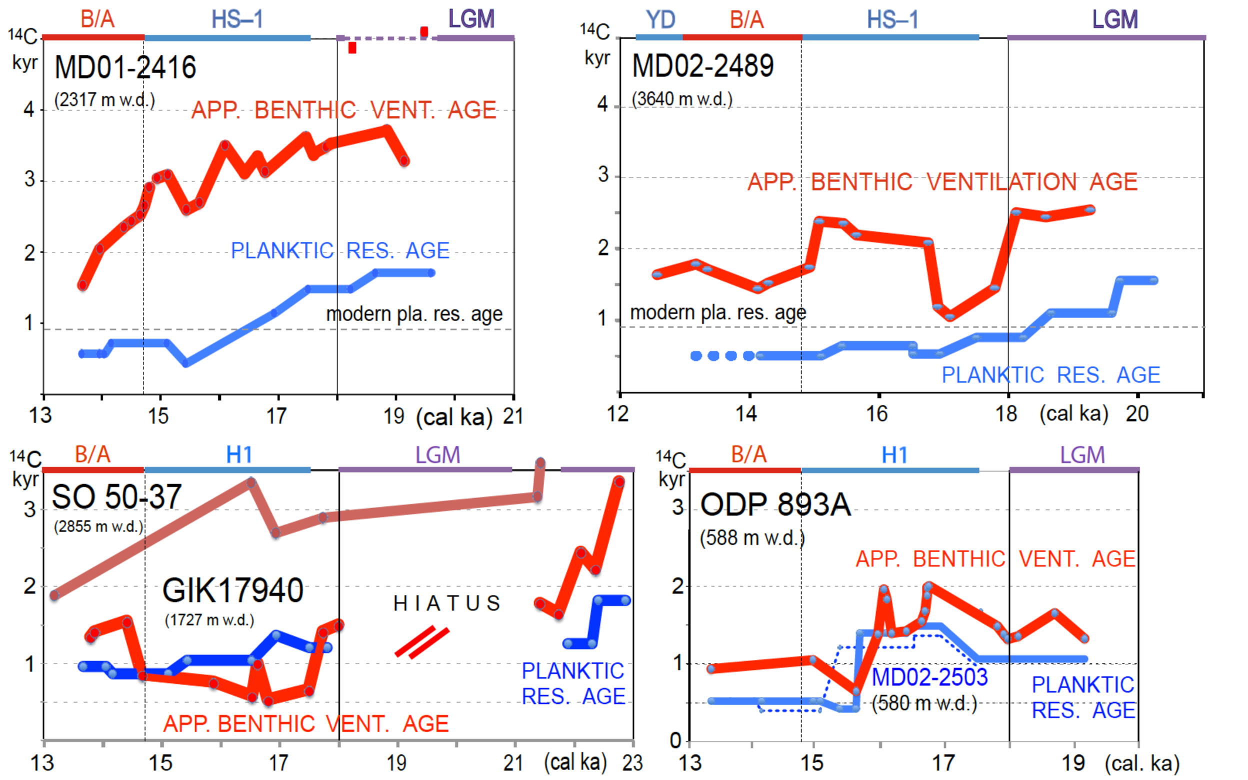

Fig. S2e. SITES in the EQUATORIAL OCEAN

CARIACO BASIN — — *SOUTHERN TIMOR SEA*

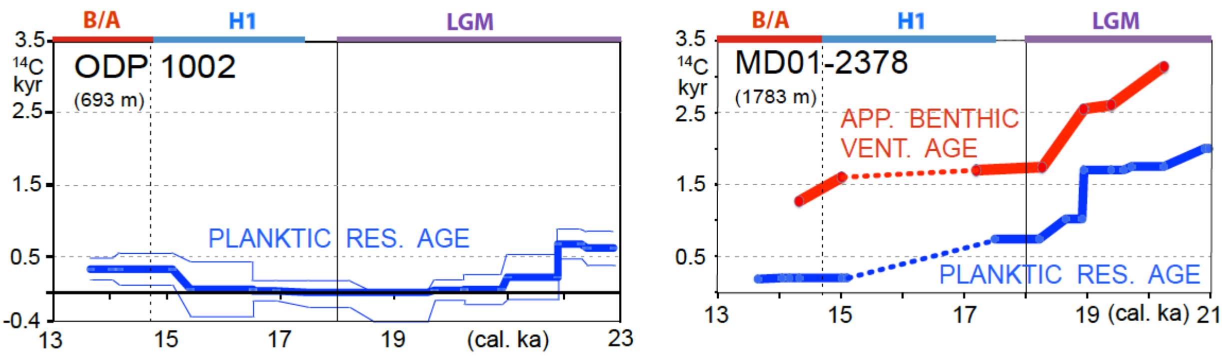

,,

,,